

Department of Physics, Chemistry and Biology

Master's Thesis

Search for Dark Matter in the Upgraded High Luminosity LHC at CERN

**Sensitivity of ATLAS phase II upgrade to dark matter
production**

Sven-Patrik Hallsjö

Thesis work performed at Stockholm University

Linköping, June 4, 2014

LITH-IFM-A-EX--14/2863--SE



Linköpings universitet
TEKNISKA HÖGSKOLAN

Search for Dark Matter in the Upgraded High Luminosity LHC at CERN

Sensitivity of ATLAS phase II upgrade to dark matter production


Sven-Patrik Hallsjö

Thesis work performed at Stockholm University

Linköping, June 4, 2014

Supervisor: **Docent Christophe Clément**
FYSIKUM Stockholm University
Professor Magnus Johansson
IFM, Linköping University

Examiner: **Professor Magnus Johansson**
IFM, Linköping University

	Avdelning, Institution Division, Department Theoretical physics group Department of Physics, Chemistry and Biology SE-581 83 Linköping	Datum Date 2014-06-04
---	---	--

Språk Language <input type="checkbox"/> Svenska/Swedish <input checked="" type="checkbox"/> Engelska/English <input type="checkbox"/> _____	Rapporttyp Report category <input type="checkbox"/> Licentiatavhandling <input checked="" type="checkbox"/> Examensarbete <input type="checkbox"/> C-uppsats <input type="checkbox"/> D-uppsats <input type="checkbox"/> Övrig rapport <input type="checkbox"/> _____	ISBN _____ ISRN LITH-IFM-A-EX--14/2863--SE Serietitel och serienummer ISSN Title of series, numbering _____
--	---	---

URL för elektronisk version http://urn.kb.se/resolve?urn=urn:nbn:se:liu:diva-XXXXX	
---	--

Titel Title	Sökandet efter mörk materia i den uppgraderade hög luminositets LHC i CERN Search for Dark Matter in the Upgraded High Luminosity LHC at CERN
Undertitel Subtitle	Känslighet hos den fas II uppgraderade ATLAS för mörk materia produktion. Sensitivity of ATLAS phase II upgrade to dark matter production
Författare Author	Sven-Patrik Hallsjö

Sammanfattning Abstract	<p>The LHC at CERN is now undergoing an set of upgrades to increase the center of mass energy for the colliding particles to be able to explore new new physical processes. The focus of this thesis lies on the so called phase II upgrade which will preliminarily be completed in 2023. After this upgrade the LHC will be able to accelerate proton beams to such velocity that each proton has a center of mass energy of 14 TeV.</p> <p>One disadvantage of this is that it will be harder for the ATLAS detector to isolate unique particle collisions since more and more collisions will occur simultaneously, so called pile-up.</p> <p>For 14 TeV there does not exist a full simulation of the ATLAS detector. This thesis instead uses simulated data for the particle collisions and then uses so called smearing functions to emulate the detector responses.</p> <p>This thesis focuses on how a mono-jet analysis looking for different WIMP models of dark matter will be affected by this increase in pile-up rate.</p> <p>The models which are in focus are thoes which try to explain dark matter without adding new theories to the standard model or QFT, such as the effective theory D5 operator and light vector mediator models.</p> <p>The exclusion limits set for the D5 operators mass suppression scale at 14 TeV and 1000 fb⁻¹ are 2-3 times better than previous results at 8 TeV and 10 fb⁻¹.</p> <p>For the first time limits have been set on which mediator masses can be excluded for vector mediator models at 14 TeV.</p>
-----------------------------------	--

Nyckelord Keywords	ATLAS, Beyond standard model physics, CERN, Dark matter, Effective operator, Elementary particle physics, High energy physics, Mono-jet analysis, Vector mediator, WIMPS.
------------------------------	---

Abstract

The LHC at CERN is now undergoing an set of upgrades to increase the center of mass energy for the colliding particles to be able to explore new new physical processes. The focus of this thesis lies on the so called phase II upgrade which will preliminarily be completed in 2023. After this upgrade the LHC will be able to accelerate proton beams to such velocity that each proton has a center of mass energy of 14 TeV.

One disadvantage of this is that it will be harder for the ATLAS detector to isolate unique particle collisions since more and more collisions will occur simultaneously, so called pile-up.

For 14 TeV there does not exist a full simulation of the ATLAS detector. This thesis instead uses simulated data for the particle collisions and then uses so called smearing functions to emulate the detector responses.

This thesis focuses on how a mono-jet analysis looking for different WIMP models of dark matter will be affected by this increase in pile-up rate.

The models which are in focus are thoes which try to explain dark matter without adding new theories to the standard model or QFT, such as the effective theory D5 operator and light vector mediator models.

The exclusion limits set for the D5 operators mass suppression scale at 14 TeV and 1000 fb^{-1} are 2-3 times better than previous results at 8 TeV and 10 fb^{-1} .

For the first time limits have been set on which mediator masses can be excluded for vector mediator models at 14 TeV.

Acknowledgments

A big thank you to my family, fiancée and friends who have supported me throughout my education. A warm thank you to my friend Joakim Skoog who altered some of the images for me.

Linköping, June 2014
Sven-Patrik Hallsjö

Contents

37	Notation	ix
38	1 Introduction	1
39	1.1 Research goals	2
40	1.2 Theoretical Background	3
41	1.2.1 Quantum mechanics and quantum field theory	3
42	1.2.2 Nuclear, particle and subatomic particle physics	4
43	1.2.3 The standard model of particle physics	4
44	1.2.4 Dark matter	5
45	1.2.5 Signal models	7
46	1.2.6 Jets	8
47	1.2.7 Search for WIMPS	8
48	1.3 Experimental overview	10
49	1.3.1 LHC	10
50	1.3.2 ATLAS	11
51	1.3.3 Coordinate system	12
52	1.3.4 Pile-up	12
53	1.3.5 Mono-jet analysis	13
54	1.3.6 Phase II high luminosity upgrade	14
55	1.3.7 Monte Carlo simulation	15
56	2 Validation of smearing functions	17
57	2.1 Smearing functions	18
58	2.1.1 Electron and photon	19
59	2.1.2 Muon	19
60	2.1.3 Tau	19
61	2.1.4 Jets	19
62	2.1.5 Missing Transverse Energy	20
63	2.2 Validation	21
64	2.2.1 Method	21
65	2.3 Results	22
66	2.3.1 Electron and photon	23
67	2.3.2 Muon	24

68	2.3.3	Tau	24
69	2.3.4	Jets	25
70	2.3.5	Missing Transversal Energy	26
71	2.3.6	Summary	27
72	2.4	Discussion	28
73	2.4.1	Dependence of smearing on pile-up	28
74	2.4.2	Comparison to expected results	28
75	2.5	Conclusion	29
76	3	Evaluating dark matter signals	31
77	3.1	Signal to background ratio	32
78	3.1.1	Signal Region	32
79	3.1.2	Weight	32
80	3.1.3	Verification of background normalization	32
81	3.1.4	Errors in data	33
82	3.1.5	Figure of merit	33
83	3.1.6	D5 operator models	35
84	3.1.7	Light vector mediator models	35
85	3.2	Signal region definitions	36
86	3.2.1	Signal regions	36
87	3.2.2	Verifying background data	36
88	3.3	Mitigating the effect of the high luminosity	36
89	3.4	Results	37
90	3.4.1	Verifying background data	37
91	3.4.2	Events	37
92	3.4.3	Limit on M^*	39
93	3.4.4	Limit on mediator mass	41
94	3.5	Discussion	43
95	3.5.1	Comparison to previous results	43
96	3.5.2	Effect of the high luminosity	43
97	3.6	Conclusion	44
98	3.6.1	Limit on M^*	44
99	3.6.2	Limit on mediator mass	44
100	3.6.3	Effect of the high luminosity	44
101	4	Final remarks	45
102	A	Datasets	49
103	A.1	Background processes	49
104	A.1.1	Validation	49
105	A.1.2	Background to signals	49
106	A.2	Signals	50
107	A.2.1	Qcut	50
108	A.2.2	D5 signal processes	50
109	A.2.3	Light vector mediator processes	50
110		Bibliography	53

111
112

Notation

NOTATIONS

113

Notation	Explanation
barn(b)	1 barn(b)= 10 ⁻²⁴ cm ²
\oplus	$a \oplus b = \sqrt{a^2 + b^2}$, $a \oplus b \oplus c = \sqrt{a^2 + b^2 + c^2}$

ABBREVIATIONS

114

Abbreviation	Expansion
ATLAS	A large Toroidal LHC ApparatuS
CERN	Organisation européenne pour la recherche nucléaire ¹
CMS	Compact Muon Solenoid
CR	Control Region
LHC	Large Hadron Collider
MC	Monte Carlo
RMS	Root Mean Square
SM	the Standard Model of particle physics
SR	Signal Region
WIMP	Weakly Interacting Massive Particle
WIMPS	Weakly Interacting Massive ParticleS
QED	Quantum ElectroDynamics
QFT	Quantum Field Theory
QM	Quantum Mechanics

¹Originally, Conseil Européen pour la Recherche Nucléaire

1

Introduction

Discrepancies in measurements of the rotations of galaxies indicate the presence of a large amount of matter which interacts through gravity, though not electromagnetically making it invisible to our telescopes. This matter is commonly referred to as dark matter. Since no known or hypothesized particle in the standard model of particle physics can be used as a candidate for dark matter, this hints at the presence of new physics.

At the Organisation Européenne pour la Recherche Nucléaire (CERN) focus lies among other things to discover any evidence of so called weakly interacting massive particles (WIMPS) which may be a candidate for dark matter. It is impossible to electromagnetically detect any interaction of dark matter candidates on the subatomic scale. However through using existing theoretical frameworks as templates to design searches by searching for assumed decay channels and by investigating what is invisible to the ATLAS and CMS detectors. By using momentum conservation it is hoped that signs will be found. Though to date no candidates for WIMPS have been found nor any other explanation of dark matter.

Current experiments at CERN and current theories now show that higher energies are required at the LHC to be able to see any signs of WIMPS. This is why the LHC and all detectors are undergoing a vast upgrade program [1]. In this thesis focus will be on the last part of the upgrade due for completion in 2023, known as the high luminosity-LHC phase II upgrade; and also on the ATLAS detector. The method used in this thesis focuses on looking at data which emulate conditions at the upgraded LHC.

1.1 Research goals

This research took place at Stockholm University from January 7th until May 16th. During the research period the following tasks were set up and performed or answered:

- Implement a C++ programme that loops over the collisions inside the signal and background datasets.
- For each collision retrieve the relevant observables (variables used to extract the signal over the background) and apply "smearing functions" to emulate the effect of the high luminosity on the observables.
- For both signal and background datasets, compare observables before and after smearing. What observables are the least/most affected?
- Implement selection criteria that selects the signal collisions efficiently while reduces significantly the background. In a first step the selection criteria should be taken from existing studies.
- Selection criteria can be evaluated and compared with each other using a figure of merit p , that measures the sensitivity of the experiment to the dark matter signal. Calculate p for the given selection criteria before and after smearing.
- What is the effect of the high luminosity (smearing) on the value of p ?
- Investigate other selection criteria and observables, to mitigate the effect of high luminosity. Use p to rank different criteria after smearing.
- Conclude on the effect of the high luminosity on the sensitivity for dark matter and possible ways to mitigate its effects using alternative observables and selection criteria.

1.2 Theoretical Background

1.2.1 Quantum mechanics and quantum field theory

In the beginning of the 20th century, some physical phenomena could not be explained by classical physics, for example the ultra-violet disaster of any classical model of black-body radiation, and the photoelectric effect [2]. It was these phenomena that led to the formulation of quantum mechanics (QM), where energy transfer is quantized and particles can act as both waves and particles at the same time [3].

Combining QM with classical electromagnetism proved harder than expected, colliding a photon(em-field) and an electron (particle/wave) is quite tricky. This can be seen when trying to calculate the scattering between them both in a QM schema. One idea that came from this was to explain them both in the same framework, field theory. Also, trying to incorporate special relativity into QM suggested a field description where space-time is described using the metric formalism from differential geometry. The culmination of both of these problems is the first part of a Quantum field theory (QFT), Quantum electrodynamics (QED) which with incredible precision explains electromagnetic phenomena including effects from special relativity [4]. It is in this merging that antimatter was theorised, since it is a requirement for the theory to hold. After the discovery of antimatter, QED was assumed to give a correct description of the phenomena around us. Since then the theory has been altered somewhat to explain more and more experimental data. This is discussed more in subsection 1.2.2 and subsection 1.2.3.

To be able to calculate properties in QFT one uses the Lagrangian formalism [5], which gives a governing equation for the different physical processes. In general the Lagrangian used for the Standard model is quite complicated, one can thus focus on one of the different terms corresponding to a specific interaction. This can be done to calculate the so called cross-section for a process.

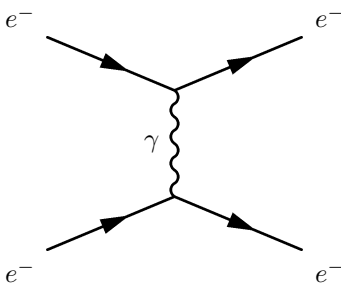


Figure 1.1: An example of a Feynman diagram explaining an electron-electron scattering using QED.

For a particle collision [6], the cross-section can be seen as a measure of the effective surface area seen by the impinging particles and as such is expressed in units of area. The cross section is proportional to the probability that an interaction will occur. It also provides a measure of the strength of the interaction between the scattered particle and the scattering center. A step to simplify the

calculation of the cross-sections is to use so called Feynman diagrams, an example of which is given in figure 1.1. Through the figure, which comes with certain rules, and knowing what the major process (in this case QED) one can calculate the cross-section [4, 6]. It is this which is needed to predict the detection of new particles.

1.2.2 Nuclear, particle and subatomic particle physics

Many could argue that these branches of physics started after Ernest Rutherford famous gold foil experiment [7], where he discovered that matter is composed of matter with a nucleus, a lot of empty space and electrons.

It was this that sparked the curiosity to see what the nucleus is made of and what forces govern the insides of atoms. After this, and the combination of the theoretical description given by QM, a lot more has been discovered and still more has been predicted. The newest of these is of course the Higgs particle, which was predicted through QFT and then discovered by the ATLAS and the CMS experiments at CERN [8, 9].

It is now known that all discovered particles are built up of fundamental particles, it is that that builds up the standard model [7].

1.2.3 The standard model of particle physics

To date there are two fundamental types of particles which are modelled as point like, quarks and leptons, seen in figure 1.2. Aside from this and also seen in the figure are the gauge bosons which are carriers of the different forces.

All other known particles are built up by these fundamental particles. These combined particles are often divided into different groups depending on the fundamental particles that build them up. For instance, particles build up of three quarks are known as hadrons. Particles with an integer spin are known as bosons whereas half-integer particles are known as fermions.

The standard model of particle physics, referred to simply as the standard model (SM), is a model which tries to categorize all the fundamental particles that have been discovered experimentally. QFT explains the interactions between these particles and it has also predicted several particles by including symmetries [7].

SM is today the pinnacle of particle physics and can be used to explain almost everything that occurs around us. There are however some problems [11]:

- There is no link between gravity and the SM.
- Asymmetry between matter and antimatter can not be fully explained.
- No explanation that can contain dark matter.

In this thesis focus lies with dark matter, some more introduction to possible dark matter and different candidates in extensions to SM are explained in subsection 1.2.4.

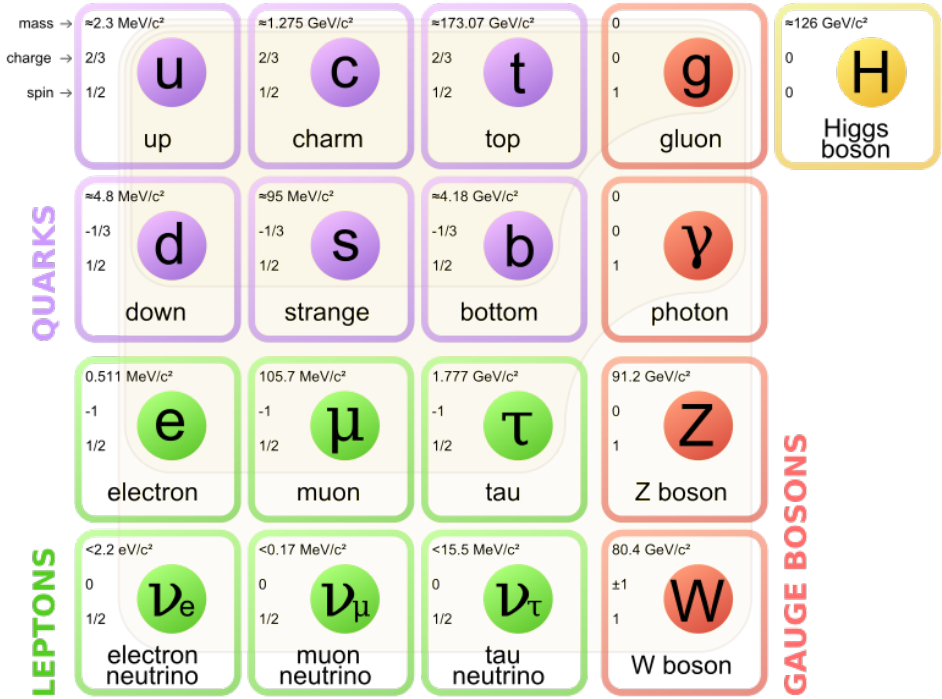


Figure 1.2: The standard model of particle physics where the three first columns represent the so called generations, starting with the first [10].

1.2.4 Dark matter

Dark matter is the name given to, among other things, the solution to the discrepancies of galactic rotations [12].

The presence of dark matter can be measured indirectly from its gravitational effects. Focus on matter in a galaxy which are rotating around the center of the galaxy. Through Newtons law of gravity and the centrifugal force one can calculate the rotation speed as a function of the distance to the center of the galaxy. Since one of these forces is attractive and the other repulsive, if the matter is in a stable orbit around the galactic center they must be equal and give us an expression for the speed depending on the distance. Newtons law can be written as the following:

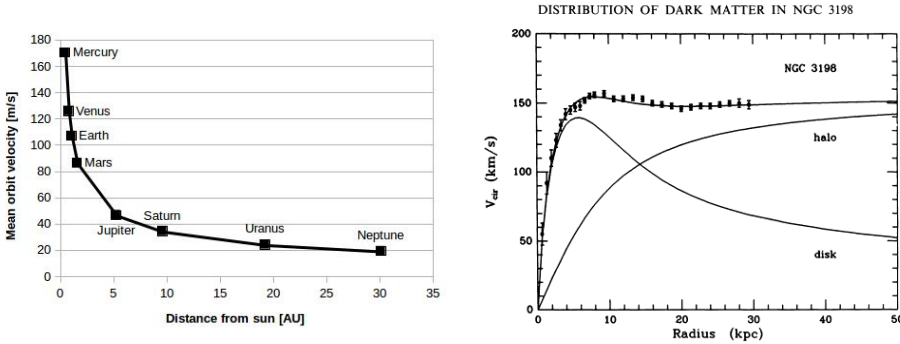
$$F_{Gravitational} = G \frac{Mm}{r^2} \equiv G_M \frac{m}{r^2} \quad F_{Centrifugal} = m \frac{V^2}{r} \quad (1.1)$$

where G is the gravitational constant, M the mass of the centre object, m the mass of the matter, r the distance between the two and V is the rotation speed. It has been simplified using G_M since all matter orbits the same galactic center. The assumption that the two objects have spherical symmetrical mass distributions

and that the rotating object is assumed in a circular orbit outside of the center object have been made. Setting the equations in (1.1) results in:

$$G_M \frac{m}{r^2} = m \frac{V^2}{r} \Leftrightarrow V^2 = \frac{G_M}{r} \Rightarrow V = \sqrt{\frac{G_M}{r}} \propto \frac{1}{\sqrt{r}} \quad (1.2)$$

where the speed is assumed to be positive and \propto means proportional. Through these simple calculations it is shown that the rotation speed should decrease with and increased distance. The same reasoning can be applied to our solar system where this is the case figure 1.3a. The relation in these units is $V = \frac{107}{\sqrt{r}}$ where 107 can be used in (1.2) to calculate the mass of the sun. However when looking at galaxies, this is not the case! In figure 1.3b experimental data can be seen from the galaxy NGC3198 with a fitted curve which does not decrease with the distance but is instead constant. This is the discrepancy which is solved by postulating the existence of dark matter [13]. After this the big question arises, what



(a) Rotation speed of planets in our solar system. Since the distance is quite small on an astronomical scale, there is no sign of dark matter. Based on data from Ref. [14].

(b) Rotation speed of matter in NGC3198 with a curve fitting and three different models, if only a dark model halo existed, if there was no dark matter and the correct, if both exist [15].

Figure 1.3: Different rotation curves, both for planets in our solar system and matter in the NGC3198 galaxy.

could this dark matter consist of? What is known so far lies in the name. It is called dark since there is no electromagnetic interaction and matter since it has gravitational interaction. This means that it can not be made up of anything in the Standard Model apart from neutrinos. Astrophysical measurements have also indicated that dark matter can not be fully explained as being neutrinos nor baryonic matter [16]. This means that dark matter can not be made out of any standard model particles.

The main interest of this thesis and also the main contributor to the rotational discrepancies is known as cold dark matter. This is due to the matter having a low speed, thus low kinetic energy, and have a high particle mass (In the GeV

scale) [11, 17, 18]. There are several strategies to search for dark matter, [11]

- Ordinary matter interacting with ordinary matter can produce dark matter, known as production. This is the processes that occurs at particle accelerators is the method explored in this thesis.
- Dark matter interacting with ordinary matter can produce dark matter, known as direct detection.
- Dark matter interacting with dark matter can produce ordinary matter, known as indirect detection.

In this thesis the focus lies with production at colliders, namely the LHC. There are several theories models for how to detect dark matter in proton-proton collisions such that occur at the LHC at CERN. This is covered more in subsection 1.2.7.

1.2.5 Signal models

In quantum field theory the objective is usually to find the part of the Lagrangian which explains a type of interaction, known as the operator of the interaction and also to find the probability amplitude (cross-section) for a certain interaction. For complicated processes it is easier to employ a simplified phenomenological model. This is done by using an effective field theory and the concept is explained in figure 1.4. The operator can be found through assuming the possible interactions and using the effective field theory [4].

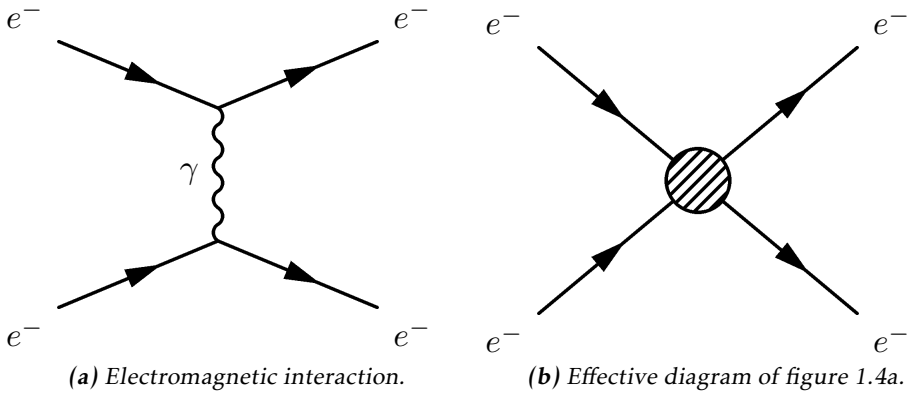
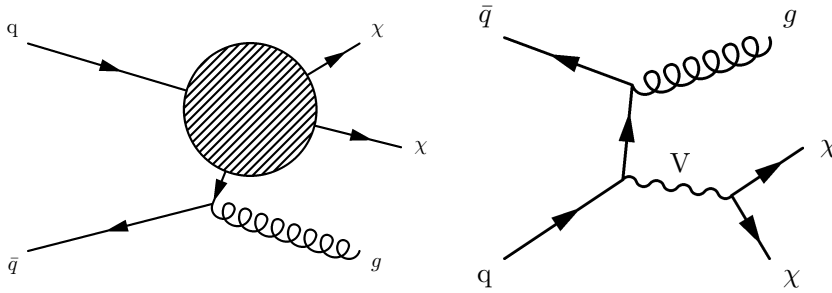


Figure 1.4: Feynman diagram of an electron-electron scattering, both as a diagram where a photon is exchanged and as its effective theory version, where the details are hidden in the blob.

In this thesis the same effective field theory as in Refs. [17, 19] is considered, denoted D5 and explained in figure 1.5a. The WIMP (denoted χ) is assumed to be the only particle in addition to the standard model fields and is assumed to interact through the electroweak force. In order to explain dark matter the WIMP

χ must be stable, for this reason only Feynman diagrams with an even number of χ are considered. It is assumed that the mediator is heavier than the WIMPs, meaning that the mediator interactions are in higher order terms of the effective field theory and thus not included in the operators. In this work, WIMPs are assumed to be Dirac fermions (half integer spin and is not its own antiparticle).

Another model which is considered is a vector mediator model which is described by figure 1.5b. This model is based on the assumption that the interaction of WIMPs is mediated by a particle denoted V which is a spin 1 particle. This particle is modelled as a heavy z -boson which governs the electroweak interactions. The free parameters of this mediator particle are its weight and its width which is related to the lifetime of the particle and which decay modes exist. It contains the same assumptions about the WIMPs as the D5 operator.



(a) Effective Feynman diagram explaining the D-operators.

(b) Feynman diagram describing the vector mediator model.

Figure 1.5: Feynman diagrams describing the signal models used in this thesis.

1.2.6 Jets

In particle collisions free gluons and quarks with high energy can be produced. According to QFT these can not exist and must decay through a process known as hadronization meaning that they will decay into a cone of energetic hadrons, which is known as a Jet. It is not possible to measure these free gluons or quarks, however this cone of hadrons will travel in the same direction and will be measured by the calorimeters, see subsection 1.3.2. These measurements can then be summed to calculate the energy and momentum which the initial gluon or quark had which in turn results in more information about the collision.

1.2.7 Search for WIMPS

The main problem with searching for WIMPS is that one is looking for a small signal among a lot of uninteresting proton-proton collisions. One way to search for WIMPS and overcome this difficulty is a so called mono-jet analysis which is described in subsection 1.3.5.

This method is a way to detect WIMP production among other proton-proton collision events and relies on the observation of high energetic jet, which arises from the gluon in both figures in figure 1.5, on one side and seemingly non conservation of energy or momentum, which will be denoted missing energy. This means that something has happened which the detectors can not detect. If the models from subsection 1.2.5 can explain the missing energy, then evidence for WIMP production would have been found.

Since the search for WIMPS at the LHC is based on looking at the missing energy, not actual detection, the experiment can not establish if a WIMP is stable on a cosmological time scale and thus if it is a dark matter candidate [18]. This means that if a candidate is found, it may still not be the dark matter that is needed to explain the cosmological observations.

ATLAS has looked at proton-proton collisions, with 8 TeV center of mass energy, which contain high energetic jets without finding any excess of mono-jet events. This is why it is very interesting that the LHC is undergoing a upgrade that will allow higher energy levels, see subsection 1.3.6. With this the processes can be given higher energy and thus the produced particles can be comprised of higher mass.

1.3 Experimental overview

1.3.1 LHC

The large hadron collider (LHC) is a particle accelerator located at CERN near Geneva in Switzerland, see figure 1.6. The accelerator was built to explore physics beyond the standard model and to make more accurate measurements of standard model physics. Before it was shut down for an upgrade in 2012 it was able to accelerate two proton beams to such a velocity that each proton in them had an energy of 4 TeV which gives a center of mass energy of $\sqrt{s} = 8$ TeV. The proton beam is comprised of bunches of protons with enough spacing that bunch collisions can happen independent of each other. The rate at which the accelerator produces a certain process can be calculated through the instantaneous luminosity. For the LHC the instantaneous luminosity was $10^{34} \text{ cm}^{-2}\text{s}^{-1}$ [20] or $10\text{nb}^{-1}\text{s}^{-1}$ where $1 \text{ barn(b)} = 10^{-24} \text{ cm}^2$.

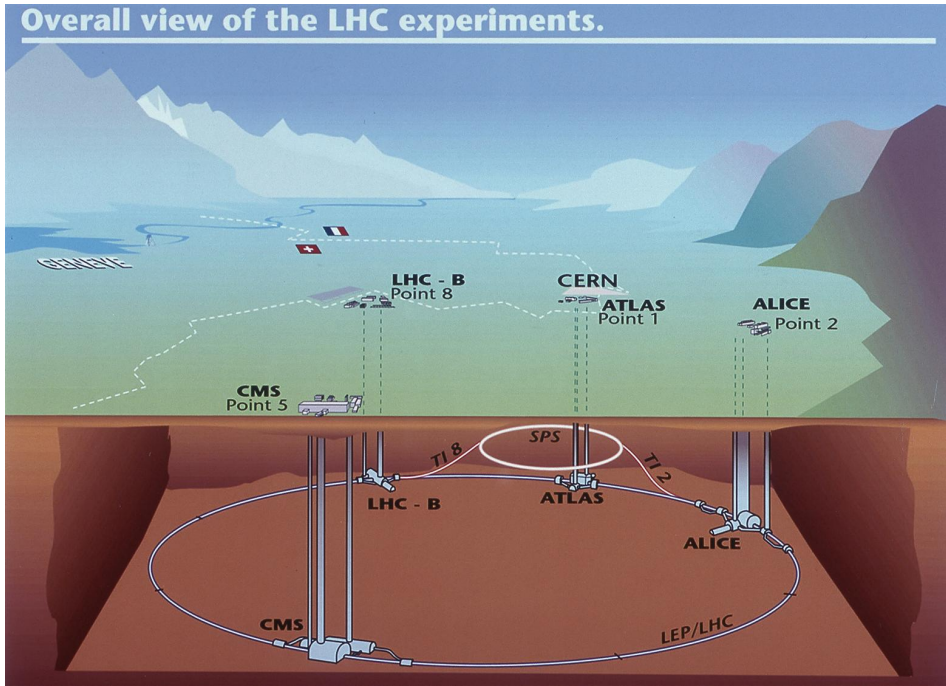


Figure 1.6: Figure showing the LHC and the different detector sites[21].

The instantaneous luminosity, often just denoted luminosity, can be defined in different ways depending on how the collision takes place. For two collinear intersecting particle beams it is defined as:

$$\mathcal{L} = \frac{fkN_1N_2}{4\pi\sigma_x\sigma_y} \quad (1.3)$$

where N_i are the number of protons in each of the bunches, f is the frequency at which the bunches collide, k the number of colliding bunches in each beam, and σ_x (σ_y) is the horizontal (vertical) beam size at the interaction point. Since the instantaneous luminosity increases quadratically with more protons in each bunch, increasing the number of protons would be a good strategy to increase the instantaneous luminosity. However aside from the difficulties to create and maintain a beam with more particles, a large N_i increases the probability for multiple collisions per bunch crossing, referred to as pile-up. Pile up will be a key aspect which is described more in subsection 1.3.4.

The expected number of events for a given physics process can be calculated by using the instantaneous luminosity, (1.3), through the following:

$$N = \sigma \int \mathcal{L} dt \equiv \sigma \mathcal{L} \quad (1.4)$$

where \mathcal{L} is the integrated luminosity and σ is the cross section which is often measured in barn. The integrated luminosity is a measurement of total number of proton-proton interactions that have occurred over time and is also a common measure of how much data was recorded. Before the LHC was shut down \mathcal{L} was 20.8 fb^{-1} .

1.3.2 ATLAS

As seen in figure 1.6, there are several detectors at the LHC. One of these is ATLAS which is a general purpose detector that uses a toroid magnet. Its goal is to observe several different production and decay channels. The detector is composed of three concentric sub-detectors, the Inner detector, the Calorimeters and the Muon spectrometer [22].

The Inner detectors main task is to measure the tracks of the particles and measures position of the initial proton-proton collision. Aside from this it measures the track momenta and the charge of charged particles. It can however only detect charged particles.

The Calorimeters, electromagnetic and hadronic, are used to measure the energy contained in the different particles. The electromagnetic calorimeter is used to measure energy and direction of photons and electrons whereas the hadronic calorimeter is designed to measure the energy and direction of hadrons.

The Muon spectrometer is used to measure signs of muons, which will simply pass through the other detectors without leaving a trace. It also measures the energy and momentum of the muons.

The neutrinos escape the ATLAS experiment without being detected, and in this thesis it is assumed that WIMPS pass through all the detectors without leaving any trace.

Therefore WIMPS and neutrinos have the same detector signature. As seen in section 3.4 the main background to the WIMP signal is the production of a Z boson that in turn decay to two neutrinos mimicking the WIMP signature.

1.3.3 Coordinate system

The coordinate system of ATLAS, seen in figure 1.7 is a right-handed coordinate system with the x-axis pointing towards the centre of the LHC ring, and the z-axis along the tunnel/beam (counter clockwise) seen from above. The y-axis points upward. The origin is defined as the geometric center of the detector. A cylindrical coordinate system is also used for the transverse plane, (R, ϕ, Z) . For simplicity the pseudorapidity of particles from the primary vertex is defined as:

$$\eta = -\ln\left(\tan \frac{\theta}{2}\right) \quad (1.5)$$

where θ is the polar angle (xz-plane) of the particle direction measured from the positive z-axis. The difference in η of two particles is through this definition invariant under Lorentz boosts in the z-direction.

It is quite common to calculate the distance between particles and jets in the (η, ϕ) space, $d = \sqrt{(\Delta\eta)^2 + (\Delta\phi)^2}$.

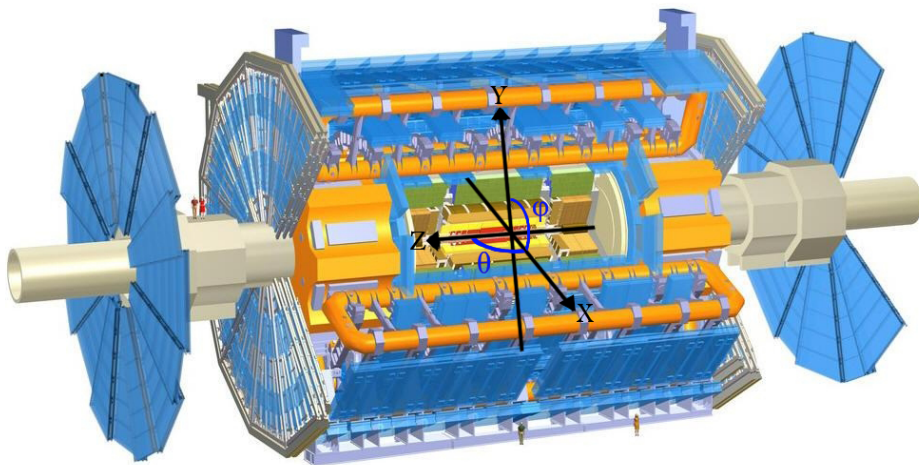


Figure 1.7: The ATLAS detector and the definition of the orthogonal Cartesian coordinate system. Image altered from Ref. [23]

1.3.4 Pile-up

Pile-up is the phenomena that several proton-proton collisions occur simultaneously. The number of pile-up is defined as the average number of proton-proton collisions that occur per bunch crossing per second. It is denoted as $\langle\mu\rangle$. μ can be calculated by adjusting a Poisson distribution to fit the curve created by the number of interactions per bunch crossing at a given luminosity. When this is done μ will be the mean value of the Poisson distribution. The value of μ will be higher for after the proposed upgrade compared to now, see section 1.3.6 which may decrease the detector performance.

1.3.5 Mono-jet analysis

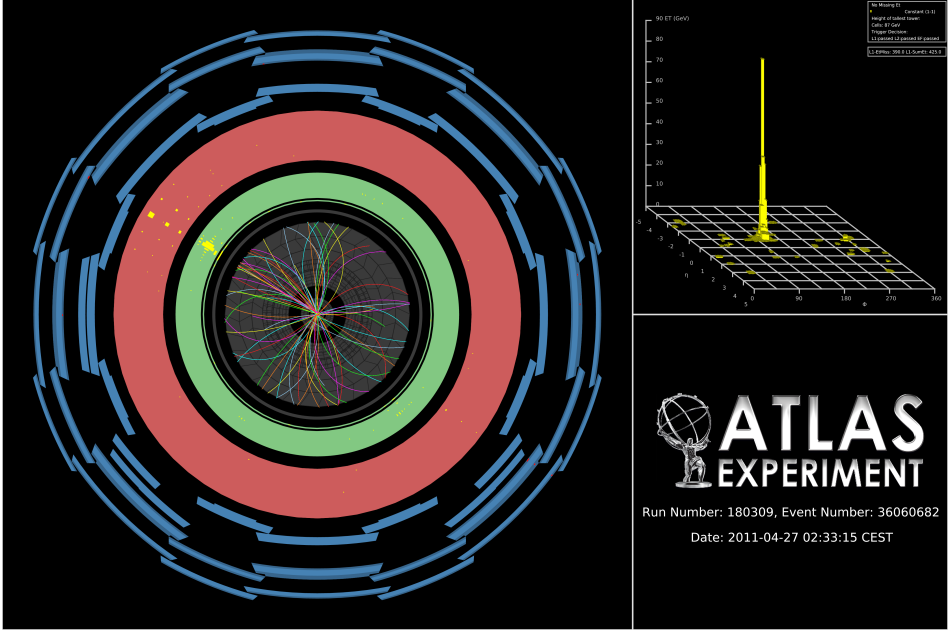


Figure 1.8: Image in the transverse plane of a mono-jet event recorded by the ATLAS experiment [24]. The figure in the top right is a diagram in the (η, ϕ) -plane showing where in the calorimeter (red in the main figure) the energy is deposited and how much.

When measuring the transverse energy one can in some interactions find inconsistencies such as jets, discussed in subsection 1.2.6, that are in excess in one direction. Conservation of momentum in the transverse plane of the experiment indicates that the sum of all momenta should be zero as before the collision. In figure 1.8 one can see a high energetic jet which gives an excess of transverse energy in one direction after the collision. Since there is no balancing jet there must be transverse energy that is not detected, denoted E_T^{Miss} . This gives an indication that the energy to balance this can not be detected. This could for instance be neutrinos or the characteristic signature of WIMPS.

E_T^{Miss} is the modulus of the E_T^{Miss} vector which is defined as:

$$\vec{E}_T^{Miss} = - \sum \vec{p}_T^{Jet} - \sum \vec{p}_T^{Electron} - \sum \vec{p}_T^{Muon} - \sum \vec{p}_T^{Tau} - \sum \vec{p}_T^{Photon} \quad (1.6)$$

where p_T denotes the transverse momenta. There are two main classes of events, signal and background. The signal corresponds to events that would arise from one of the processes in subsection 1.2.5. However to know that the missing energy is sign of the signal then one must understand all the other components that could contribute to the missing energy. Also there must be an excess of missing energy from what is expected from the background.

The background comprises of standard model processes that can mimic the mono-jet signature.

1.3.6 Phase II high luminosity upgrade

At the moment, the whole LHC is undergoing a step by step upgrade program which be finalized around 2022-2023, denoted the high luminosity upgrade, or HL-upgrade. The upgrade consists of different stages, meaning that the upgrade will halt for periods so that experiments can take place. In figure 1.9 one can see

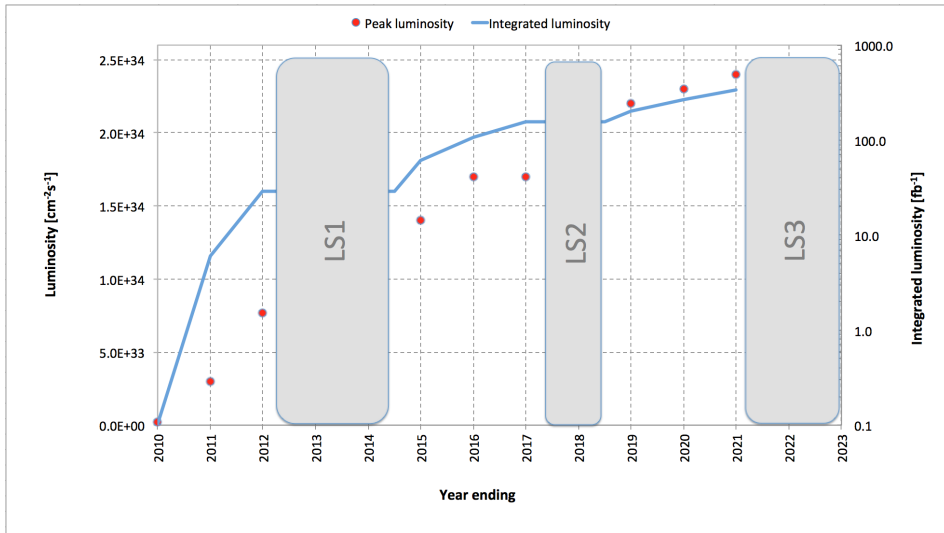


Figure 1.9: A graph showing the upgrading timetable with the instantaneous luminosity, denoted luminosity, and integrated luminosity expected in the different stages.

the three proposed upgrades. The period after LS1 is denoted phase 0, after LS2 phase I and after LS3 phase II.

LS1 is the upgrade which will take the LHC to its designed performance.

LS2 will push the LHC to the ultimate designed instantaneous luminosity without too dramatic changes to the accelerator.

LS3 which is the focus of this thesis, will increase the instantaneous luminosity even more. Though for this to happen a modification of the whole LHC must be done, instead of just an upgrade and maintenance as before.

The following is expected for the experiments done after phase II:

Entity	Expected	Last run (2012)
Instantaneous luminosity	$\mathcal{L} \sim 50 \text{ nb}^{-1} \text{ s}^{-1}$	$\mathcal{L} \sim 10 \text{ nb}^{-1} \text{ s}^{-1}$
Integrated luminosity	$\mathcal{L} = 1000 - 3000 \text{ fb}^{-1}$	$\mathcal{L} = 20 \text{ fb}^{-1}$
Pile-up	$\langle \mu \rangle = 140$	$\langle \mu \rangle = 20$
Center of mass energy	$\sqrt{s} = 14 \text{ TeV}$	$\sqrt{s} = 8 \text{ TeV}$

Table 1.1: Expected running values for the Phase II HL-upgraded LHC with older values for comparison [25].

Where it should be noted that the integrated luminosity indicates the total amount of data which will be collected after the upgrade is completed before the next upgrade takes place.

1.3.7 Monte Carlo simulation

As mentioned before, in this thesis only emulated data has been used. This data is created by using a Monte Carlo (MC) simulation of the background processes and the expected signal. To do this a program called MadGraph is used.

MadGraph [26] starts with Feynman diagrams and then generates simulated events based on lots of different parameters. This generator was used to generate signal samples used in this thesis.

Sherpa, [27] is very similar to MadGraph and was used to generate the background samples used in this thesis.

PYTHIA [28] is a package which adds the correct description of jets to MadGraph by including hadronization. The correct description of pile-up comes from other ATLAS software.

The tool to access all this data and analyse it a tool called ROOT, which is used for programming high energy physics related tools [29].

Validation of smearing functions

A full detector simulation of the ATLAS detector based on the GEANT [30] program makes it possible to obtain the expected detector responses to electrons, muons, tau leptons, photons (γ) and jets of hadrons. However these simulations are extremely time-consuming and require a lot of computing power. Also at the present time only a limited set of these simulations exists for the ATLAS phase II upgrade.

In this thesis a different strategy is used. Instead of performing a full detector simulation the observed particles from the event generator, which simulates the proton-proton collisions, are smeared by using random numbers following resolution functions specific to each type of particle. These emulate how the detector and the reconstruction is affected by the increased luminosity and the pile-up which comes with this.

The resolution functions or smearing functions are the official functions developed from previous studies [1, 31] by the ATLAS collaboration for the study of the ATLAS phase II upgrade. The key result of those studies was that the direction of the momenta is unaffected and that only jets and E_T^{Miss} are affected by pile-up. Since this was confirmed in previous studies it was not incorporated into the smearing functions as discussed more in section 2.1.

Since part of this thesis work is to take the official ATLAS smearing functions and apply the smearing to each particle, it is important to check that the energy and momenta resolutions of the smeared objects are consistent with the expected values. Thus in this chapter the energy and momenta resolutions are measured after applying the smearing to some simulated processes and the resulting resolutions are compared with the expected values.

2.1 Smearing functions

In a simulation of a proton-proton collision all quantities such as energy, momentum and direction of all produced particles are perfectly known. In a real experiment it is only possible to get measured values from the detector. The detector energy and momentum resolutions given in the smearing functions relate the measured values to the true values on a statistical basis. To emulate the measured energies and momenta, their true values are smeared using the known detector resolutions.

The smearing functions are designed so that they take into account the efficiency of the different detectors, how they are constructed as well as their dependence on pile-up. The functions are dependent on the measured entries energy or momenta.

Terminology:

- Data before smearing, simulated data, is denoted as data at a truth level or truth data.
- Data after smearing, which is comparable to what is measured is denoted as reconstructed data.

Observable	Absolute σ
Electron & photon	$\sigma = 0.3 \oplus 0.1 \sqrt{E(\text{GeV})} \oplus 0.01 E(\text{GeV}), \eta < 1.4$ $\sigma = 0.3 \oplus 0.15 \sqrt{E(\text{GeV})} \oplus 0.015 E(\text{GeV}), 1.4 < \eta < 2.47$
Muon momentum	$\sigma = \frac{\sigma_{id} \sigma_{ms}}{\sigma_{id} \oplus \sigma_{ms}}$ $\sigma_{id} = p_T (a_1 \oplus a_2 p_T)$ $\sigma_{ms} = p_T (\frac{b_0}{p_T} \oplus b_1 \oplus b_2 p_T)$
Tau energy	$\sigma = (0.03 \oplus \frac{0.76}{\sqrt{E(\text{GeV})}}) E(\text{GeV}), \text{ for 3 prong.}$
Jet momentum	$\sigma = p_T (\text{GeV}) (\frac{N}{p_T} \oplus \frac{S}{\sqrt{p_T}} \oplus C)$ where $N = a(\eta) + b(\eta)\mu$
E_T^{Miss}	$\sigma = (0.4 + 0.09 \sqrt{\mu}) \sqrt{\sum E(\text{GeV})} + 20\mu$

Table 2.1: Expected absolute σ where the parameters are given for muons in table 2.2 and for jets in table 2.3. Functions take from Ref. [31].

	a_1	a_2	b_0	b_1	b_2
$ \eta < 1.05$	0.01607	0.000307	0.24	0.02676	0.00012
$ \eta > 1.05$	0.03000	0.000387	0.00	0.03880	0.00016

Table 2.2: Parameters used in the muon smearing function taken from Ref. [31].

$ \eta $	a	b	S	C
0-0.8	3.2	0.07	0.74	0.05
0.8-1.2	3.0	0.07	0.81	0.05
1.2-2.8	3.3	0.08	0.54	0.05
2.8-3.6	2.8	0.11	0.83	0.05

Table 2.3: Parameters used in the jet smearing function taken from Ref. [31].

2.1.1 Electron and photon

The identification of electrons relies on finding an isolated electron track and a pattern in the calorimeter compatible with an electron shower. Pile-up will affect the electrons by decreasing the efficiency to identify an electron because of the increased number of tracks. However for the identified electrons the energy resolution will be close to that without pile-up.

The electron and photon have the same smearing since they are both detected in a similar way.

2.1.2 Muon

The identification of muons relies on isolated tracks in the inner detector being matched with information in the muon system. Since the muon system is the outer most detector seen from the collision point it is hardly effected by the effects of pile-up.

2.1.3 Tau

Tau is detected similarly to electron and photon. In this thesis all tau processes are for simplicity assumed to be at 3 prong. Where prong refers to the different amount of tracks from which they were reconstructed. This in turn means that the effect of pile-up will be worse compared to an electron as a triplet must be found in an increased number of tracks.

2.1.4 Jets

Jets as described in subsection 1.2.6 as a cone of hadronic particles.

527 The largest effect of pile-up is to add additional jets in the ATLAS detector. These
 528 additional jets contribute to additional energy deposited inside the existing jets
 529 and to E_T^{Miss} .

530 **2.1.5 Missing Transverse Energy**

531 E_T^{Miss} , the missing transverse energy, which was discussed in subsection 1.3.5,
 532 and defined in (1.6) is calculated by knowing that there should be energy conser-
 533 vation in the collision. In is comprised of different parts, one from neutrinos, one
 534 from errors in the other measurements and one from new physics. It should be
 535 affected by pile-up as described above.

2.2 Validation

To validate the smearing functions a comparison with Ref. [31] was made where the standard deviation, depending on the energy or momentum value of an process, is given in table 2.5. This is performed using the simulated processes listed in table 2.4.

Particle	Process
Electron	$W \rightarrow e \nu$
Muon	$W \rightarrow \mu \nu$
Tau	$W \rightarrow \tau \nu$
γ	γ + jet sample
Jets	jet sample
E_T^{Miss}	$Z \rightarrow \nu \nu$ + jet sample

Table 2.4: Different processes from where data has been taken. Each sample is a simulation of a physical process, the simulation names can be found in appendix A

2.2.1 Method

The energy and momentum resolutions are obtained for each type of particle by comparing the values before and after smearing.

By fitting a Gaussian curve of the smeared data from a given energy or momenta value will then result in the standard deviation which is used in the validation. The standard deviation is also known as the resolution of the data and will be denoted σ and not cross-section as in chapter 1

The standard deviation is then compared to previous results [31].

To get good statistics enough data must be available for a given truth energy or momenta. Aside from this the analysis must be specific enough to only look at a narrow enough interval around this point.

The method is presented step by step below:

- Take a MC sample with a given particle, i.e electrons.
- Choose electrons which have a truth energy of 75 GeV.
- Plot the smeared electron energy for this value of truth energy. These plots are given for electrons and photons in figure 2.1.
- Fit a gauss function to the distribution of smeared energy and from this retrieve the sigma value of the fit.
- Compare the measured sigma to the expected resolution given from the smearing functions.

2.3 Results

As discussed above, the method was to plot the data against its smeared counterpart and through this determine σ to see if it conforms to the expected values.

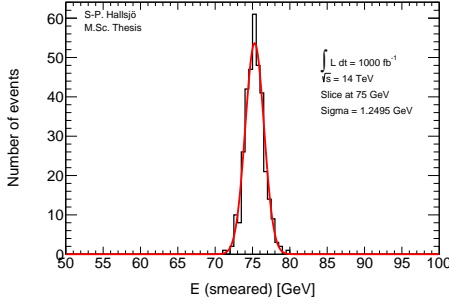
Only one energy or momenta value is shown for simplicity, though the comparison was done for different energy values. The energy is denoted E and in the figures momenta is denoted P_T for transverse momenta.

The average number of pile-up, explained in subsection 1.3.4, is fixed at 60 as a benchmark unless anything else is stated.

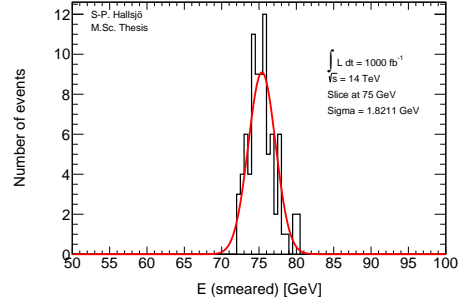
As in the comparison, figure 2.1, figure 2.2, figure 2.4 and figure 2.5 are divided depending on the different η values.

2.3.1 Electron and photon

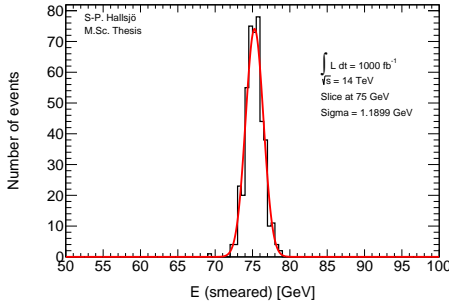
Since these interact very similarly in the detector, their smearing functions are identical. The slice value represents at which value of unsmeared energy or momentum this smearing occurs. In figure 2.1 the Gaussian fit (red) and the data (black) are given for the electron energies.



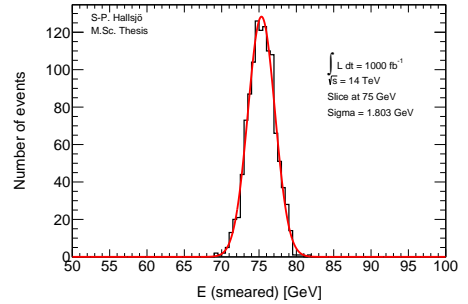
(a) Electron energy after smearing for $|\eta| < 1.4$.



(b) Electron energy after smearing for $1.4 < |\eta| < 2.47$.



(c) Photon energy after smearing for $|\eta| < 1.4$.

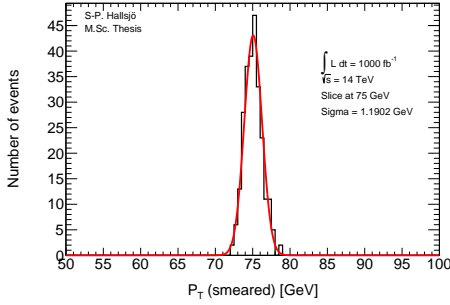


(d) Photon energy after smearing for $1.4 < |\eta| < 2.47$.

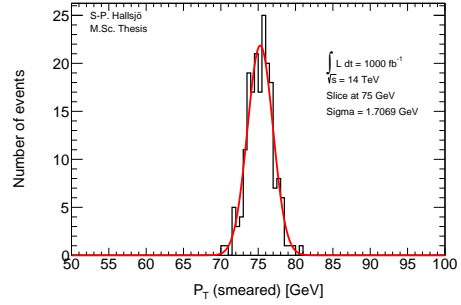
Figure 2.1: Photon and electron energy after smearing.

2.3.2 Muon

Since muons are shielded from the effects of pile-up only efficiency and detector limitations affect the smearing. In figure 2.2 the Gaussian fit (red) and the data (black) are given for the muon momenta.



(a) Muon momenta after smearing for $|\eta| < 1.05$.

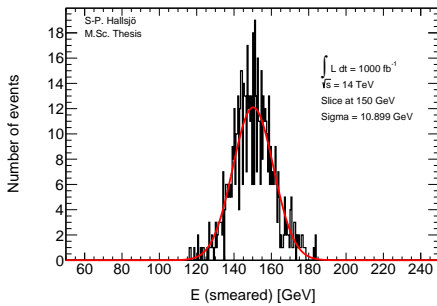


(b) Muon momenta after smearing for $1.05 < |\eta|$.

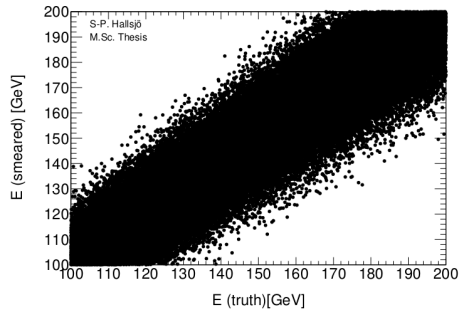
Figure 2.2: Muon momenta after smearing.

2.3.3 Tau

As described in subsection 2.1.3 taus are detected similarly to electrons and photons. Thus the plots should look similarly to those in the previous subsection apart from the slice being at 150 GeV. In figure 2.3a the Gaussian fit (red) and the data (black) are given for tau detected through 3 prong. In figure 2.3b smeared versus truth energy is shown.



(a) Tau energy after smearing.

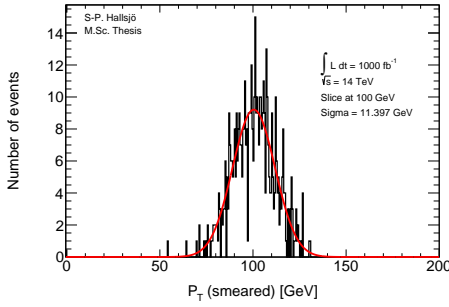


(b) Tau energy vs smeared.

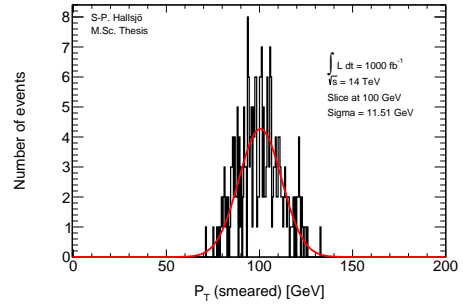
Figure 2.3: Tau energy after smearing and energy vs smearing.

2.3.4 Jets

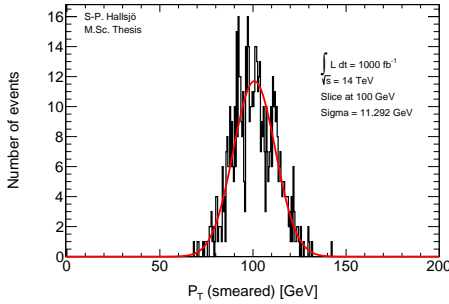
The smearing functions are divided into four different regions depending on the angle η .



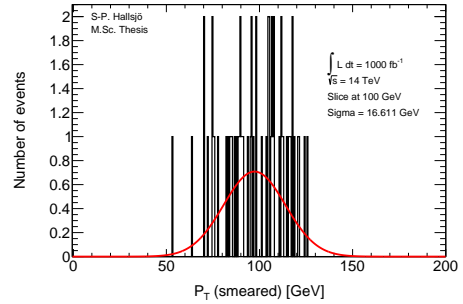
(a) Jet momenta after smearing for $|\eta| < 0.8$.



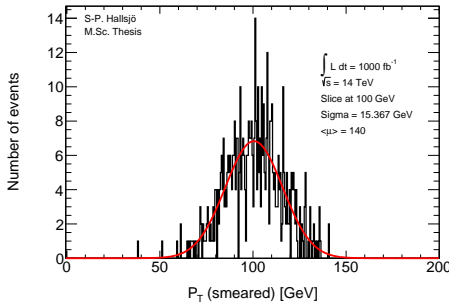
(b) For $0.8 < |\eta| < 1.2$.



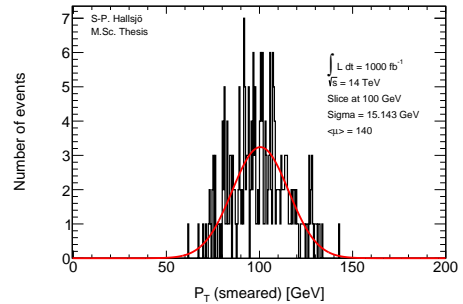
(c) Jet momenta after smearing for $1.2 < |\eta| < 2.8$.



(d) For $2.8 < |\eta| < 3.6$. Very odd due to the low amount of available data.



(e) Jet momenta after smearing for $|\eta| < 0.8$ at $\langle\mu\rangle = 140$.



(f) For $0.8 < |\eta| < 1.2$ at $\langle\mu\rangle = 140$.

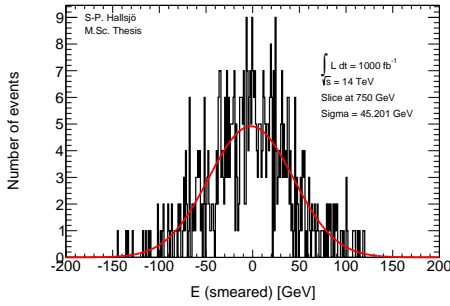
Figure 2.4: Jet momenta after smearing.

In figure 2.4 the Gaussian fit (red) and the data (black) are given for the jet momenta. Where $\langle\mu\rangle$ is the average number of simultaneous proton-proton collisions as explained in subsection 1.3.4.

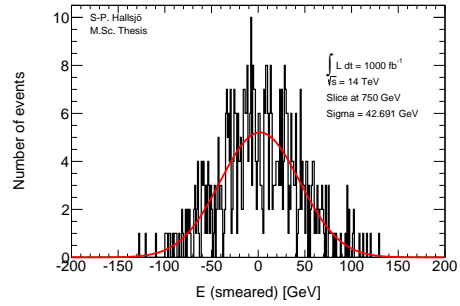
2.3.5 Missing Transversal Energy

The figures in this subsection are, compared to the above, given as absolute smearing, thus at 0 it represents that the energy is unsmeared, compared to the others where the slice value represents the unsmeared.

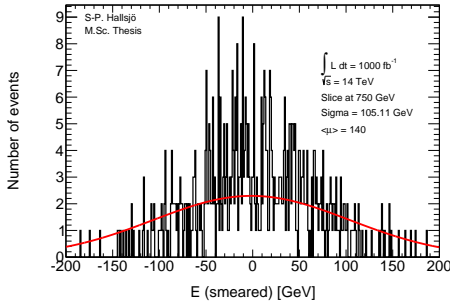
Here the E_T^{Miss} is projected down to the x- and y-axis, since these are the transverse axes, to be smeared.



(a) E_T^{Miss} smearing along the x-axis.



(b) E_T^{Miss} smearing along the y-axis.



(c) E_T^{Miss} smearing along the y-axis for $\langle\mu\rangle = 140$.

Figure 2.5: E_T^{Miss} smearing plots

2.3.6 Summary

Since the leptons and photons are all detected by fitting detectors responses to different tracks, meaning that the effect of pile-up should be that there are more track to match, but it should not affect which ones are matched. The independence of pile-up for leptons and photons is backed up in previous research, for instance [1, 32].

To validate the smearing code, comparisons are made with [31] which gave table 2.1 for the expected σ . Where p_T denotes the transverse momenta, E the energy and μ the pile-up value. The subscripts id and ms for the muon momentum resolution denote the parametrisation of the inner detector and the muon spectrometer.

Process	σ [GeV]	Expected σ [GeV]
Electron low η	1.25 ± 0.05	1.18
High η	1.82 ± 0.14	1.74
Photon low η	1.19 ± 0.04	1.18
High η	1.80 ± 0.04	1.74
Muon low η	1.19 ± 0.05	1.50
High η	1.71 ± 0.09	2.18
Tau	10.9 ± 0.3	10.3
Jet low η	11.4 ± 0.4	11.6
$\langle \mu \rangle = 140$	15.4 ± 0.5	15.8
Mid low η	11.5 ± 0.5	11.9
$\langle \mu \rangle = 140$	15.1 ± 0.7	15.9
Mid high η	11.3 ± 0.3	10.9
High η	16.6 ± 1.5	13.5
E_T^{Miss}	43 ± 2	48
$\langle \mu \rangle = 140$	105 ± 12	87

Table 2.5: Calculated σ values compared to expected σ given from the resolution given in table 2.1.

- Where the given σ is still the absolute.
- Where the large difference between calculated and expected σ for Muons and E_T^{Miss} is explained by to optimistically calculated errors in σ .

2.4 Discussion

2.4.1 Dependence of smearing on pile-up

From the validation done it is interesting to note that the smearing functions were created from previous studies [1, 32], had shown that detector resolution for leptons and photons is unaffected by pile-up. This may seem unexpected however it becomes quite logical when one understands how the detectors work. To be able to detect particles the detectors must detect an excess of energy which comes from a particle passing through. The amount of particles passing through will of course increase, but the detections should be unaffected as well as the recreation of the events. However with the same logic it makes sense that jets and E_T^{Miss} are quite affected since they are combined of several parts, either hadronic particles or by all the transverse missing energy.

Another interesting part is how the effect diminishes with an increasing energy. As seen above, and through the the formulas in table 2.1, for the high energies which are of interest here the effect of pile-up minimal.

2.4.2 Comparison to expected results

One of the major problems in the comparison was to get the significance of the Gaussian fit to be calculated correctly. The tool ROOT has a lot of different features which made this task somewhat difficult, specifically calculating optimistic errors. Also large contribution is that this is a statistical property and thus there is a statistical fluctuation in the result.

Another problem was to retrieve the correct resolution values from Ref. [31], since it was unclear if the resolution values given were absolute or scale dependent. This has now been corrected in a new version of the paper.

2.5 Conclusion

The smearing functions work as intended within 5.8 sigma, however when using a test box and averaging the sigmas one ends up with half of this for the extreme cases, muons and E_T^{Miss} y-axis. This means indicated that the statistical fluctuation of these values and in the error calculations is considerable. Even with this statistical fluctuation the smearing functions work as intended.

3

Evaluating dark matter signals

The main goal of the thesis is to investigate if certain dark matter signals can be detected after the high luminosity upgrade. One immediate worry is that the background will be large in comparison to the signal, making the signal undetectable.

Another goal is to investigate if it might become more difficult to differentiate between the signal and background due to the degradation of jet and missing energy resolutions in the high luminosity upgrade.

This thesis focus on using a luminosity at 1000 fb^{-1} and a center of mass energy at 14 TeV. The reconstructed data is created using a pile-up rate, $\langle \mu \rangle = 140$ as expected during phase II.

The signal models are given in appendix A along with the background models. The different models were introduced subsection 1.2.5 and will be discussed in more detail in this chapter.

Each signal model has been evaluated in different signal regions and the detectability has been evaluated using a statistical p-value.

3.1 Signal to background ratio

3.1.1 Signal Region

A signal region (SR) is defined as a set of selections on event variables designed to create a sample which is enriched in signal and depleted of background. One usually tries to design the signal region so that the signal is large enough and the background small enough that one would statistically be able to either:

- Exclude the signal if the observation of the data is compatible with a background only hypothesis.
- Detect the signal and quantify the significance of the excess in data over background if the data is consistent with a signal + background hypothesis.

An event is a recorded proton-proton collision which consists of hundreds or thousands of observables such as the number of electrons, muons, jets, tau leptons, gammas or E_T^{Miss} each with their energy and momenta.

To define an optimal signal region is not known a priori and has to be studied for different signal models. The optimal region typically changes e.g with a change of the mass of new particles for instance the WIMP mass or the suppression scale. This is why there are several different signal regions to be studied in this thesis.

3.1.2 Weight

A weight is used to normalize different types of data so that they can be compared. As given in (1.4), the total number of events can be estimated as:

$$N = \sigma \int \mathcal{L} dt \equiv \sigma \mathcal{L} \quad (3.1)$$

Thus, if all events are generated at different luminosities, depending on the computing power of the computer which performed the simulation, the following weight should be used to receive the events at a new luminosity:

$$weight = \frac{\mathcal{L}\sigma}{N_{Raw}} \quad (3.2)$$

where N_{Raw} is the number of events expected at the luminosity that was set to create the data, compared to \mathcal{L} which is the luminosity at which the data is compared and σ is the cross-section. In this thesis the luminosity is fixed at $\mathcal{L} = 1000\text{fb}^{-1}$.

3.1.3 Verification of background normalization

To verify that the background samples are correctly normalized they are compared with Ref. [33] in which the center of mass energy is 8 TeV and the luminosity is 10fb^{-1} . Since the luminosity is not 1000fb^{-1} as used in this thesis the expected values from the paper scaled up with a factor 100 to be comparable.

Somewhat unexpectedly a center of mass energy at 8 TeV had cross-sections a factor 4 lower than the cross-sections at 14 TeV. These cross-sections are generated

either with MadGraph[26] or PYTHIA[28] depending on the generator given for each dataset in appendix A.

The signal regions used in the article were the following:

Selection Criteria		
Jet veto, require no more than 2 jets with $p_T > 30\text{GeV}$ and $ \eta < 4.5$		
Lepton veto, no electron or muon		
Leading jet with $ \eta < 2.0$ and $\Delta\phi(\text{jet}, E_T^{\text{Miss}}) > 0.5$ (second-leading jet)		
signal region	SR3p	SR4p
minimum leading jet p_T (GeV)	350	500
minimum E_T^{Miss} (GeV)	350	500

Table 3.1: The signal regions from Ref. [33].

The article [33] has in total four signal regions, unfortunately since the simulated events used in this thesis are filtered before the analysis only the two highest regions are comparable. This can be seen in table 3.3 in subsection 3.4.1.

3.1.4 Errors in data

To make a through analysis of the background it is important to take into consideration different errors that exist in the number of events. This is especially important when looking at which signals can be excluded in different signal regions. There exists three main types of errors:

- Statistical errors from MC.
- Statistical errors from the control region.
- Systematic errors.

The statistical errors from MC come from the method of generating background events and is unfortunately nothing that can be estimated when one is not generating the events.

The statistical errors from the control region require an explanation of what a control region is. A control region (CR) is similar to a signal region, a set of criteria which are imposed on the data. This criteria are set so that there can be a region with almost no signal. In this CR there will still be fluctuations in the amount of background events due to statistical effects, which can then be measured.

The systematic errors is a fixed error which is always present coming from different approximations in how all the events were generated.

3.1.5 Figure of merit

To be able to evaluate different signal regions and different signal models, a figure of merit p is used. The value p is the probability for the background to fluctuate

to the value of the signal + background. Thus if the p-value is small, regardless if the signal is large or the background or its fluctuations are small, it is improbable that the background could result in the same value as if there was a signal and background. This means that for a sufficiently small p-value the signal is detectable.

Assuming the expected number of background events are $B \pm \sigma_B$ where σ_B is the quadratic sum of the statistical error from Monte Carlo, the statistical error from the control region (CR) and the systematic errors as explained in subsection 3.1.5. The expected number of signal events is S , assumed without fluctuation.

If no uncertainty in B or S is assumed, then the probability that the background will fluctuate up to the signal and background should follow a Poisson distribution as such:

$$P(S+B|B) = \frac{e^{-B} B^{(S+B)}}{(S+B)!} \quad (3.3)$$

The probability that the background will fluctuate to a value N larger or equal to the signal and background then becomes:

$$P(B \geq S+B|B) \equiv P(N|B) = \sum_{N=S+B}^{\infty} \frac{e^{-B} B^N}{N!} \quad (3.4)$$

However since there is an uncertainty in the background, the probability distribution $P(N|B)$ must be convoluted with a Gaussian function:

$$G(N_B|B, \sigma_B) = \frac{1}{\sigma_B \sqrt{2\pi}} e^{-\frac{(N_B-B)^2}{2\sigma_B^2}} \quad (3.5)$$

where N_B is the expected number of background events. The convolution is done using N_B as B resulting in the total probability density function:

$$\begin{aligned} F(N|N_B, \sigma_B) &= P(N|B) * G(N_B|B, \sigma_B) = \\ &= \int_{-\infty}^{\infty} P(N|N_B - B) G(N_B|B, \sigma_B) dN_B \end{aligned} \quad (3.6)$$

Inserting the sum over N leads to the probability of the background fluctuation to signal and background being obtained as.

$$p = \sum_{N=S+B}^{\infty} \int_{-\infty}^{\infty} P(N|N_B - B) G(N_B|B, \sigma_B) dN_B \quad (3.7)$$

In this thesis, two different models of the error in the background σ_B are used. Both models are based on Ref. [33]. As described in the beginning of this subsection the error is calculated as:

$$\sigma_B = \text{Statistical error from MC} \oplus \text{Statistical error in CR} \oplus \text{Systematic error}$$

- The statistical error from MC has been neglected since there is no way of estimating it.
- The statistical error from background CR has been take from the article and assumed to decrease with the increased luminosity as, $\frac{30}{380} \frac{\sqrt{L_{old}}}{\sqrt{L_{new}}}$
- The systematic error has been given two different values, from the article: $\frac{30}{380}$ or fixed at 0.02.
- All this results the total error being used as either, 0.08 or 0.02.

3.1.6 D5 operator models

As described in subsection 1.2.5, one of the signals is modelled using the D5 operator. In this thesis two different scenarios are used, one at a dark matter mass of 50 GeV and one at 400 GeV.

Each of these models are modelled with a mass suppression scale, denoted M^* , which is connected to the cross-section of the process through:

$$\sigma_{new} = \frac{\sigma_{old}}{M^*} \quad (3.8)$$

where σ_{old} is the theoretically calculated sigma and σ_{new} denotes the sigma which is used taking the mass suppression scale into account. In subsection 3.4.3 it is determined which values of M^* could be excluded with the upgraded LHC phase 2 upgrade and ATLAS.

3.1.7 Light vector mediator models

As described in subsection 1.2.5, the other signal model is a vector mediator model. In this thesis these signals have two different width scenarios and a number of different mediator mass scenarios. **Where width is related to the lifetime of the dark matter particle.** In addition to this there are, as with the D5 operator, two different dark matter masses, one at 50 GeV and one at 400 GeV.

The result of the investigation of which models are excludable with the upgraded LHC phase 2 upgrade and ATLAS are given in subsection 3.4.4.

3.2 Signal region definitions

3.2.1 Signal regions

To be able to compare signal results to previous studies new signal regions were devised. It was also discovered that the requirement of no electrons or muons was too harsh for the signal models. Through these new selection criteria were devised. In table 3.2 the superscript lead denotes the entity with highest transverse momentum p_T . Thus $electron^{lead}$ would be the simulated electron in an event with the highest p_T .

Selection Criteria					
Jet veto, require no more than 2 jets with $p_T > 30\text{GeV}$ and $ \eta < 4.5$					
Lepton veto, no electron or muon.					
The electron veto is defined: $\Delta R(jet^{lead}, electron^{lead}) \geq 0.4$ and $electron^{lead} p_T > 20\text{GeV}$ removed.					
The muon veto is defined: $\Delta R(jet^{lead}, muon^{lead}) \geq 0.4$ and $muon^{lead} p_T > 20\text{GeV}$ removed.					
Leading jet with $ \eta < 2.0$ and $\Delta\phi(jet, E_T^{Miss}) > 0.5$ (second-leading jet)					
signal region	SR1	SR1p	SR2	SR3	SR4
minimum leading jet p_T (GeV)	350	500	600	800	1000
minimum E_T^{Miss} (GeV)	350	500	600	800	1000
signal region	SRa	SRb	SRc	SRd	
minimum leading jet p_T (GeV)	350	350	350	350	
minimum E_T^{Miss} (GeV)	350	600	800	1000	

Table 3.2: The new signal regions.

3.2.2 Verifying background data

To make sure that the altered electron veto still produces results comparable with [33] a comparison is made again. This can be seen in subsection 3.4.1 in table 3.4.

3.3 Mitigating the effect of the high luminosity

As discussed in subsection 2.4.1 the smearing functions effect of pile-up should be minimal in the high energy regions which are of interest in this thesis.

From the formulation of the smearing functions, the biggest effect should be seen at low energies. This is related to the difficulty for the hardware triggers to select events. This means that one drawback of the high luminosity upgrade is that very low energy signal regions will be lost.

The effect of the high luminosity is seen in chapter 3.4 and discussed in subsection 3.5.2.

3.4 Results

3.4.1 Verifying background data

In table 3.3 and table 3.4 a comparison has been made between the number of simulated background events at a truth level and the number of expected events by scaling up the values from Ref. [33] by a factor 100. Truth data was used to not let the increased pile-up value affect the comparison. It can be seen that the simulated events and expected events coincide quite well on all accounts apart from $W \rightarrow \tau \nu$, $W \rightarrow \mu \nu$ and thus the total as well.

The difference in $W \rightarrow \tau \nu$ can be explained by the fact that τ can not be recreated as a jet in the simulated events which it can in measured events.

The difference in $W \rightarrow \mu \nu$ is explained through the simulated events having a better separation of muons neutrinos and E_T^{Miss} .

Process	SR3p		SR4p	
	Simulated	From paper	Simulated	From paper
$Z \rightarrow \nu \nu$	140298	152000	25250	27000
$W \rightarrow \tau \nu$	40701	37000	5862	3900
$W \rightarrow e \nu$	11229	11200	1507	1600
$W \rightarrow \mu \nu$	13727	15800	1872	4200
Total background	205955	218000	34491	36700

Table 3.3: Comparison of the simulated and expected events from Ref. [33] with $\mathcal{L} = 1000\text{fb}^{-1}$, cross-sections corresponding to $\sqrt{s} = 8\text{TeV}$ and using the same electron and muon veto.

Process	SR1		SR1p	
	Simulated	From paper	Simulated	From paper
$Z \rightarrow \nu \nu$	150753	152000	27569	27000
$W \rightarrow \tau \nu$	49320	37000	7318	3900
$W \rightarrow e \nu$	18329	11200	2534	1600
$W \rightarrow \mu \nu$	22290	15800	3218	4200
Total background	240690	218000	40639	36700

Table 3.4: Comparison of the simulated and expected events from Ref. [33] with $\mathcal{L} = 1000\text{fb}^{-1}$, cross-sections corresponding to $\sqrt{s} = 8\text{TeV}$ and using a modified electron and muon veto.

3.4.2 Events

In the following tables the number of events are given using one of the D5 operators as the signal, and the background in the different signal regions. The number of background events is also used for the vector mediator signals.

Process at $\sqrt{s} = 14\text{TeV}$	SR1	SR2	SR3	SR4	SRa	Srb	Src	Srd
D5, mDm=50 GeV, M*=1TeV	131844	30900	11053	4532	131844	37217	13280	5387
$Z \rightarrow \nu\nu$	619752	44146	8764	2205	619752	61193	11975	2998
$W \rightarrow \tau\nu$	169983	8753	1479	344	169983	12047	2032	453
$W \rightarrow e\nu$	63026	2986	510	114	63026	4114	688	160
$W \rightarrow \mu\nu$	76618	3880	658	162	76618	5094	871	199
Total background	929379	59765	11411	2825	929379	82448	15566	3810

Table 3.5: Signal and background events for truth data in the signal regions.

Process at $\sqrt{s} = 14\text{TeV}$	SR1	SR2	SR3	SR4	SRa	Srb	SRc	Srd
D5, mDm=50 GeV, M*=1TeV	122117	28663	10273	4259	122117	39618	14151	5679
$Z \rightarrow \nu\nu$	568410	40518	8012	2023	568410	74564	13817	3318
$W \rightarrow \tau\nu$	170999	8644	1442	314	170999	16241	2446	536
$W \rightarrow e\nu$	60071	2799	470	110	60071	5366	835	183
$W \rightarrow \mu\nu$	73495	3704	629	152	73495	6622	1046	236
Total background	872975	55665	10552	2599	872975	102793	18144	4273

Table 3.6: Signal and background events for reconstructed data with $\langle\mu\rangle = 140$ in the signal regions.

799 Note how the ratio between the number of signal events and total background increases from the first to the last signal regions
800 meaning that these are good choices of signal regions. Also note how similar the two tables are even though table 3.6 is
801 reconstructed with a pile-up rate of 140.

3.4.3 Limit on M^*

For the D5 operators as described in subsection 3.1.6 limits on the mass suppression has been calculated by evaluating at which point the signal is covered by the background, meaning that the p -value > 0.05 . This is done using the two different error models as described in subsection 3.1.5 as figures of merit.

The limit is found, seen as a horizontal line in both figure 3.1 and figure 3.2, when the p -value $= 0.05$. In these images the effect of a change of error model can be seen as a left shift but no change in incline.

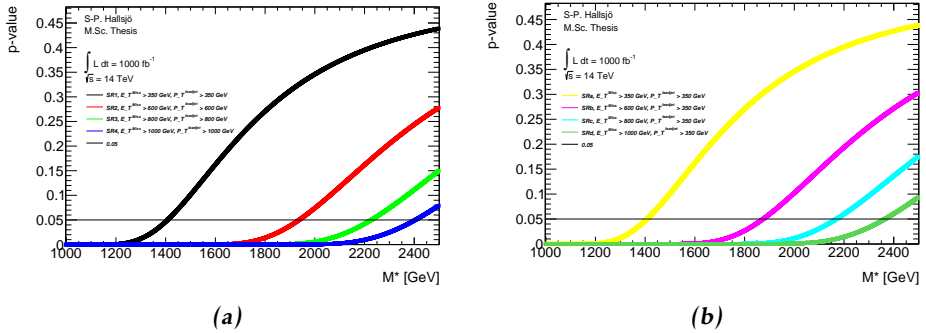


Figure 3.1: Limits of the mass suppression on a truth level for error model 0.02.

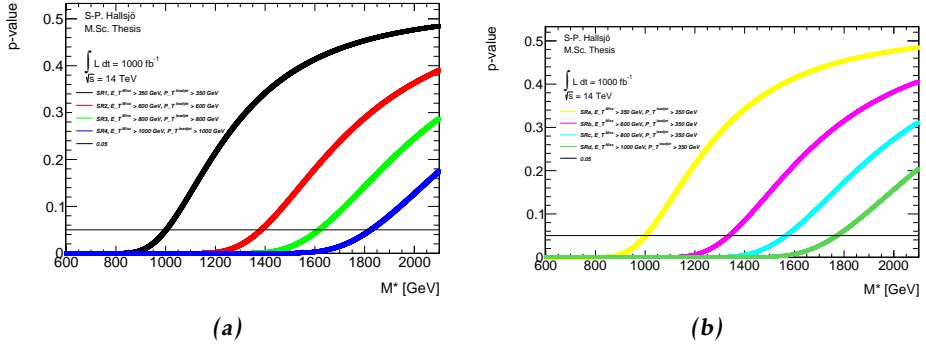


Figure 3.2: Limits of the mass suppression on a truth level for error model 0.08.

Calculating the intersection between these lines and 0.05 results in, tables 3.7-3.10 for both a dark matter mass of 50 GeV and at 400 GeV at the different error models.

Signal region	Truth [GeV]	Reco [GeV]
SR1, symmetric 350 GeV	1407	1402
SR2, 600	1936	1934
SR3, 800	2227	2226
SR4, 1000	2404	2406
SRa, symmetric 350 GeV	1425	1421
SRb, asymmetric 600 GeV	1874	1803
SRc, 800	2169	2125
SRd, 1000	2365	2340

Table 3.7: Limits on mass suppression scales in GeV given for $m_{Dm}=50$ GeV and the 0.02 error model.

Signal region	Truth [GeV]	Reco [GeV]
SR1	1002	999
SR2	1384	1382
SR3	1617	1619
SR4	1825	1834
SRa	1338	1286
SRb	1356	1303
SRc	1567	1533
SRd	1771	1745

Table 3.8: Limits on mass suppression scales in GeV given for $m_{Dm}=50$ GeV and the 0.08 error model.

Signal region	Truth [GeV]	Reco [GeV]
SR1, symmetric 350 GeV	1333	1329
SR2, 600	18481	1847
SR3, 800	2162	2163
SR4, 1000	2332	2303
SRa, symmetric 350 GeV	1350	1346
SRb, asymmetric 600 GeV	1789	1721
SRc, 800	2106	2059
SRd, 1000	2288	2258

Table 3.9: Limits on mass suppression scales in GeV given for $m_{Dm}=400$ GeV and the 0.02 error model.

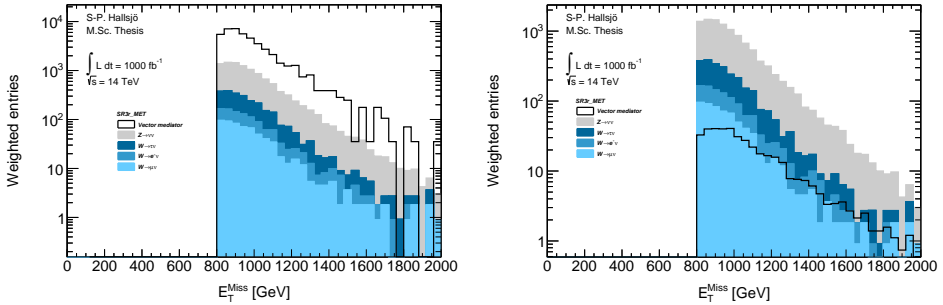
What should be noted from these tables is the significant difference between the different signals regions, especially between 4 and d which are similar apart from the lead jet momenta cut. Also how small the effect from pile-up seems to be and the increase in dark matter mass.

Signal region	Truth [GeV]	Reco [GeV]
SR1	949	946
SR2	1321	1320
SR3	1570	1573
SR4	1770	1755
SRa	961	959
SRb	1277	1228
SRc	1521	1484
SRd	1714	1684

Table 3.10: Limits on mass suppression scales in GeV given for $mDm=400$ GeV and the 0.08 error model.

3.4.4 Limit on mediator mass

For the vector mediator modes as described in subsection 3.1.7 limits on which models can be excluded have been calculated. This is done by calculating which models the p-value is < 0.05 . This is done using the two different error models as described in subsection 3.1.5 as figures of merit. All signals which have been used can be found in A.2.3.

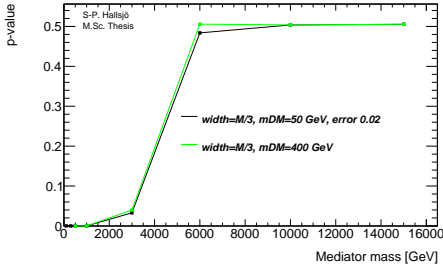


(a) A signal model given in log-scale which is not blocked by the amount of background and is thus excludable.

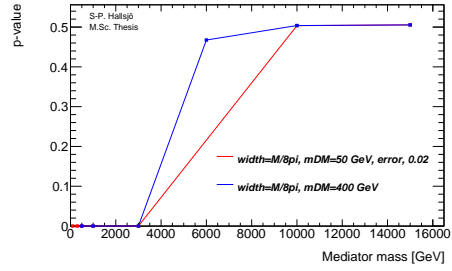
(b) A signal model given in log-scale which is blocked by the amount of background and is thus nonexcludable.

Figure 3.3: Signal on background plot for E_T^{Miss} on a reconstructed level in SR3 to illustrate a signal which is excludable and one which is not.

To set a limit on the mediator mass the p-value is calculated in different signal regions for the different signal models with different mediator mass. As an example a plot of this in signal region d is given in figure 3.4 where the p-value of the models is plotted against the increasing mediator mass for different widths and dark matter masses. The result of which models are excludable, thus with a p-value < 0.05 are given in tables 3.11 and 3.12.



(a) P-values at a reconstructed level for different mediator masses and dark matter masses at a width of $m/3$.



(b) P-values at a reconstructed level for different mediator masses and dark matter masses at a width of $m/8\pi$.

Figure 3.4: P-values at a reconstructed level for the the different mediator masses, dark matter masses and different widths which were investigated in SRd.

width	mDM=50 GeV	mDM=400 GeV
$m/3$	1000 GeV	1000 GeV
$m/8\pi$	3000 GeV	3000 GeV

Table 3.11: Limits on which the highest mediator mass which can be excluded for different widths, different dark matter masses for truth and reconstructed data and both error models. In SR2, 3, 4, c, d.

width	mDM=50 GeV	mDM=400 GeV
$m/3$	1000 GeV	1000 GeV
$m/8p$	1000 GeV	1000 GeV

Table 3.12: Limits on which the highest mediator mass which can be excluded for different widths, different dark matter masses for truth and reconstructed data and both error models. In SRb.

What can be seen in the tables is that the models are very robust when it comes to increased fluctuation in the background as indicated by the error models and with the introduction of pile-up. It is though quite interesting to see that SRb is the signal region which was worst suited for the vector mediator signals. Which by looking at the definition would suggest that the background is less susceptible to a lead jet cut than the signals.

3.5 Discussion

3.5.1 Comparison to previous results

The background was compared to Ref. [33] altering the cross-sections of the samples used in this thesis to simulate a center of mass energy of 8 TeV instead of 14. This could unfortunately not be done for the signals as that would require new samples to be produced. As seen and some what discussed in subsection 3.4.1 the events corresponded quite nicely to the values from the paper. The discrepancies are explained by general differences between simulations and measured events, such as:

- The difference in $W \rightarrow \tau \nu$ can be explained by the fact that τ can not be recreated as a jet in the simulated events which it can in measured events.
- The difference in $W \rightarrow \mu \nu$ is explained through the simulated events having a better separation of muons neutrinos and E_T^{Miss} .

Where the choice of a new muon veto giving more events supports the final claim.

In table 3.13 the limits for the mass suppression scale are given from both the paper and from this work. It is seen that the increase in luminosity and center of mass energy gives an increase of the mass suppression scale by a factor of 2-3.

Dark matter mass	From simulation	From paper
50 GeV	1960 GeV	800 GeV
400 GeV	1871 GeV	700 GeV

Table 3.13: M^* values in SR2 from both simulation at 14 TeV, 1000fb^{-1} and from Ref. [33] at 8 TeV and 10fb^{-1} .

3.5.2 Effect of the high luminosity

As seen in section 3.4, the effect of a pile-up rate of 140 is minute in the signal regions chosen. The primary focus of this thesis was to look at the effect of pile-up, and try to mitigate the effect of it. However it is shown here that by choosing signal regions with a high enough requirement the effect is minute. Thus the focus was shifted to perform a more in-depth mono-jet analysis of different Dm signal models. These models were specifically the vector mediators.

For the mass suppression scale, as seen in subsection 3.4.3, comparing the truth values against the reconstructed values the difference is at most $< 5\%$. Thus these signal regions are preferable for use in the high luminosity upgrade.

Regarding the mediator models, as discussed in subsection 3.4.4 the models are sensitive to exclusion regardless of truth or reconstructed data. This suggests that the different models are very robust or that the effect of pile-up is negligible. However the later is more probable since a tougher error model produces the same results.

3.6 Conclusion

3.6.1 Limit on M^*

The limits can be found in subsection 3.4.3 and are 2-3 times better than previous results at 8 TeV and 10fb^{-1} .

3.6.2 Limit on mediator mass

The limits can be found in subsection 3.4.4 and is the first result done with these models and thus can not be compared.

3.6.3 Effect of the high luminosity

At a pile-up level of 140 the effect is at most $< 5\%$ for the mass suppression scale and does not affect the vector mediator models which are robust as discussed in subsection 3.5.2.

4

Final remarks

In this thesis an introduction is given to phenomena in elementary particle physics, see chapter 1. After this a validation of smearing functions is done to validate that the measured resolution is compatible with what is expected, see chapter 2. In this chapter, table 2.1 contains the expected resolutions. Finally in chapter 3 two different dark matter signal models are investigated, both an effective theory and a vector mediator model.

Suggestions for future research should focus on that which would have been done if time was not an issue. With an unlimited amount of time chapter 3 would have been expanded to contain several different effective theory models and consider models which are based on Supersymmetry. Another interesting continuation would be to investigate new signal regions to see if it is possible to mitigate the effects of high luminosity even at low energies. This may be possible by using other selection criteria. Similarly it would be interesting to see if there are better selection criteria to increase the ratio of signal to background.

The most interesting continuation of this work would be to compare the results given here to measurements done after the phase II upgrade and hopefully see characteristic signatures from WIMPS.

Appendix

A

Datasets

Disclaimer: This appendix is not yet complete.

A.1 Background processes

All datasets used are d4pd which is a dataformat used at CERN.

A.1.1 Validation

For the validation the following datasets were used, with a filter at generator level at 450GeV for lead jet and MET.

157539 sherpa ct10 znunupt280 157534 sherpa ct10 wenupt200

157535 sherpa ct10 wmunupt200

157536 sherpa ct10 wtaunupt200

129160 pythia8 au2cteq6l1 perf jf17

129160 pythia8 au2cteq6l1 perf jf17

129170 pythia8 au2cteq6l1 gammajet dp17

They should be read as such: Monte Carlo version, dataset number, generator, ? name.

A.1.2 Background to signals

The same as the above though now with the filter as indicated by their name. The second znunu sample has been generated with and center of mass energy at 8 TeV.

157539 sherpa ct10 znunupt280

157539 8tev sherpa ct10 znunupt280

920 157536 sherpa ct10 wtaunupt200
 921 157534 sherpa ct10 wenupt200
 922 157535 sherpa ct10 wmunupt200

923 A.2 Signals

924 A.2.1 Qcut

925 Qcut means that the original data has been split into different parts depending
 926 on the value of the lead jet pt.

927 A.2.2 D5 signal processes

928 188408 madgraphpythia auct2bcteq6l1 d5 dm50 ms10000 qcut200
 929 188409 madgraphpythia auct2bcteq6l1 d5 dm50 ms10000 qcut400
 930 188410 madgraphpythia auct2bcteq6l1 d5 dm50 ms10000 qcut600
 931 188411 madgraphpythia auct2bcteq6l1 d5 dm400 ms10000 qcut200
 932 188412 madgraphpythia auct2bcteq6l1 d5 dm400 ms10000 qcut400
 933 188413 madgraphpythia auct2bcteq6l1 d5 dm400 ms10000 qcut600

934 All signals should be read as such: Monte Carlo version, dataset number, gen-
 935 erator, ?, name of operator, dark matter mass, default mass suppression scale,
 936 qcut part. As discussed in reference

937 A.2.3 Light vector mediator processes

938 188414 madgraphpythia auct2bcteq6l1 dm5 dm50 mm100 w3 qcut200
 939 188422 madgraphpythia auct2bcteq6l1 dm5 dm50 mm100 w3 qcut400
 940 188430 madgraphpythia auct2bcteq6l1 dm5 dm50 mm100 w3 qcut600
 941 188415 madgraphpythia auct2bcteq6l1 dm5 dm50 mm300 w3 qcut200
 942 188423 madgraphpythia auct2bcteq6l1 dm5 dm50 mm300 w3 qcut400
 943 188431 madgraphpythia auct2bcteq6l1 dm5 dm50 mm300 w3 qcut600
 944 188416 madgraphpythia auct2bcteq6l1 dm5 dm50 mm500 w3 qcut200
 945 188424 madgraphpythia auct2bcteq6l1 dm5 dm50 mm500 w3 qcut400
 946 188432 madgraphpythia auct2bcteq6l1 dm5 dm50 mm500 w3 qcut600
 947 188417 madgraphpythia auct2bcteq6l1 dm5 dm50 mm1000 w3 qcut200
 948 188425 madgraphpythia auct2bcteq6l1 dm5 dm50 mm1000 w3 qcut400
 949 188433 madgraphpythia auct2bcteq6l1 dm5 dm50 mm1000 w3 qcut600
 950 188418 madgraphpythia auct2bcteq6l1 dm5 dm50 mm3000 w3 qcut200
 951 188426 madgraphpythia auct2bcteq6l1 dm5 dm50 mm3000 w3 qcut400
 952 188434 madgraphpythia auct2bcteq6l1 dm5 dm50 mm3000 w3 qcut600
 953 188419 madgraphpythia auct2bcteq6l1 dm5 dm50 mm6000 w3 qcut200
 954 188427 madgraphpythia auct2bcteq6l1 dm5 dm50 mm6000 w3 qcut400
 955 188435 madgraphpythia auct2bcteq6l1 dm5 dm50 mm6000 w3 qcut600

956 188420 madgraphpythia auct2bcteq6l1 dmv dm50 mm10000 w3 qcut200
957 188428 madgraphpythia auct2bcteq6l1 dmv dm50 mm10000 w3 qcut400
958 188436 madgraphpythia auct2bcteq6l1 dmv dm50 mm10000 w3 qcut600

959 188421 madgraphpythia auct2bcteq6l1 dmv dm50 mm15000 w3 qcut200
960 188429 madgraphpythia auct2bcteq6l1 dmv dm50 mm15000 w3 qcut400
961 188437 madgraphpythia auct2bcteq6l1 dmv dm50 mm15000 w3 qcut600

962 188438 madgraphpythia auct2bcteq6l1 dmv dm50 mm100 w8pi qcut200
963 188446 madgraphpythia auct2bcteq6l1 dmv dm50 mm100 w8pi qcut400
964 188454 madgraphpythia auct2bcteq6l1 dmv dm50 mm100 w8pi qcut600

965 188439 madgraphpythia auct2bcteq6l1 dmv dm50 mm300 w8pi qcut200
966 188447 madgraphpythia auct2bcteq6l1 dmv dm50 mm300 w8pi qcut400
967 188455 madgraphpythia auct2bcteq6l1 dmv dm50 mm300 w8pi qcut600

968 188440 madgraphpythia auct2bcteq6l1 dmv dm50 mm500 w8pi qcut200
969 188448 madgraphpythia auct2bcteq6l1 dmv dm50 mm500 w8pi qcut400
970 188456 madgraphpythia auct2bcteq6l1 dmv dm50 mm500 w8pi qcut600

971 188441 madgraphpythia auct2bcteq6l1 dmv dm50 mm1000 w8pi qcut200
972 188449 madgraphpythia auct2bcteq6l1 dmv dm50 mm1000 w8pi qcut400
973 188457 madgraphpythia auct2bcteq6l1 dmv dm50 mm1000 w8pi qcut600

974 188442 madgraphpythia auct2bcteq6l1 dmv dm50 mm3000 w8pi qcut200
975 188450 madgraphpythia auct2bcteq6l1 dmv dm50 mm3000 w8pi qcut400
976 188458 madgraphpythia auct2bcteq6l1 dmv dm50 mm3000 w8pi qcut600

977 188444 madgraphpythia auct2bcteq6l1 dmv dm50 mm10000 w8pi qcut200
978 188452 madgraphpythia auct2bcteq6l1 dmv dm50 mm10000 w8pi qcut400
979 188460 madgraphpythia auct2bcteq6l1 dmv dm50 mm10000 w8pi qcut600

980 188445 madgraphpythia auct2bcteq6l1 dmv dm50 mm15000 w8pi qcut200
981 188453 madgraphpythia auct2bcteq6l1 dmv dm50 mm15000 w8pi qcut400
982 188461 madgraphpythia auct2bcteq6l1 dmv dm50 mm15000 w8pi qcut600

983 188462 madgraphpythia auct2bcteq6l1 dmv dm400 mm500 w3 qcut200
984 188468 madgraphpythia auct2bcteq6l1 dmv dm400 mm500 w3 qcut400
985 188474 madgraphpythia auct2bcteq6l1 dmv dm400 mm500 w3 qcut600

986 188463 madgraphpythia auct2bcteq6l1 dmv dm400 mm1000 w3 qcut200
987 188469 madgraphpythia auct2bcteq6l1 dmv dm400 mm1000 w3 qcut400
988 188475 madgraphpythia auct2bcteq6l1 dmv dm400 mm1000 w3 qcut600

989 188464 madgraphpythia auct2bcteq6l1 dmv dm400 mm3000 w3 qcut200
990 188470 madgraphpythia auct2bcteq6l1 dmv dm400 mm3000 w3 qcut400
991 188476 madgraphpythia auct2bcteq6l1 dmv dm400 mm3000 w3 qcut600

992 188465 madgraphpythia auct2bcteq6l1 dmv dm400 mm6000 w3 qcut200
993 188471 madgraphpythia auct2bcteq6l1 dmv dm400 mm6000 w3 qcut400
994 188477 madgraphpythia auct2bcteq6l1 dmv dm400 mm6000 w3 qcut600

995	188466	madgraphpythia	auet2bcteq6l1	dmv	dm400	mm10000	w3	qcut200
996	188472	madgraphpythia	auet2bcteq6l1	dmv	dm400	mm10000	w3	qcut400
997	188478	madgraphpythia	auet2bcteq6l1	dmv	dm400	mm10000	w3	qcut600
998	188467	madgraphpythia	auet2bcteq6l1	dmv	dm400	mm15000	w3	qcut200
999	188473	madgraphpythia	auet2bcteq6l1	dmv	dm400	mm15000	w3	qcut400
1000	188479	madgraphpythia	auet2bcteq6l1	dmv	dm400	mm15000	w3	qcut600
1001	188480	madgraphpythia	auet2bcteq6l1	dmv	dm400	mm500	w8pi	qcut200
1002	188486	madgraphpythia	auet2bcteq6l1	dmv	dm400	mm500	w8pi	qcut400
1003	188492	madgraphpythia	auet2bcteq6l1	dmv	dm400	mm500	w8pi	qcut600
1004	188481	madgraphpythia	auet2bcteq6l1	dmv	dm400	mm1000	w8pi	qcut200
1005	188487	madgraphpythia	auet2bcteq6l1	dmv	dm400	mm1000	w8pi	qcut400
1006	188493	madgraphpythia	auet2bcteq6l1	dmv	dm400	mm1000	w8pi	qcut600
1007	188482	madgraphpythia	auet2bcteq6l1	dmv	dm400	mm3000	w8pi	qcut200
1008	188488	madgraphpythia	auet2bcteq6l1	dmv	dm400	mm3000	w8pi	qcut400
1009	188494	madgraphpythia	auet2bcteq6l1	dmv	dm400	mm3000	w8pi	qcut600
1010	188483	madgraphpythia	auet2bcteq6l1	dmv	dm400	mm6000	w8pi	qcut200
1011	188489	madgraphpythia	auet2bcteq6l1	dmv	dm400	mm6000	w8pi	qcut400
1012	188495	madgraphpythia	auet2bcteq6l1	dmv	dm400	mm6000	w8pi	qcut600
1013	188484	madgraphpythia	auet2bcteq6l1	dmv	dm400	mm10000	w8pi	qcut200
1014	188490	madgraphpythia	auet2bcteq6l1	dmv	dm400	mm10000	w8pi	qcut400
1015	188496	madgraphpythia	auet2bcteq6l1	dmv	dm400	mm10000	w8pi	qcut600
1016	188485	madgraphpythia	auet2bcteq6l1	dmv	dm400	mm15000	w8pi	qcut200
1017	188491	madgraphpythia	auet2bcteq6l1	dmv	dm400	mm15000	w8pi	qcut400
1018	188497	madgraphpythia	auet2bcteq6l1	dmv	dm400	mm15000	w8pi	qcut600

Bibliography

- 1021 [1] Collaboration ATLAS. Letter of Intent for the Phase-II Upgrade of the
1022 ATLAS Experiment. Dec 2012. URL [https://cds.cern.ch/record/](https://cds.cern.ch/record/1502664/)
1023 1502664/. Cited on pages 1, 17, 27, and 28.
- 1024 [2] B.H. Bransden and C.J. Joachain. *Quantum mechanics*. Pearson Education,
1025 second edition, 2000. Cited on page 3.
- 1026 [3] S-P. Hallsjö. Covering the sphere with noncontextuality inequalities.
1027 Bachelor's thesis, Linköping University, The Institute of Technology,
1028 2013. URL [http://urn.kb.se/resolve?urn=urn:nbn:se:liu:](http://urn.kb.se/resolve?urn=urn:nbn:se:liu:diva-103663)
1029 diva-103663. Cited on page 3.
- 1030 [4] A. Zee. *Quantum Field Theory in a Nutshell*. Princeton University Press,
1031 illustrated edition edition, March 2003. ISBN 0691010196. Cited on pages
1032 3, 4, and 7.
- 1033 [5] H. Goldstein, C. P. Poole, and J. L. Safko. *Classical Mechanics (3rd Edition)*.
1034 Addison-Wesley, 3 edition, June 2001. ISBN 0201657023. Cited on page 3.
- 1035 [6] W. Herr and B. Muratori. Concept of luminosity. 2006. URL <http://cds.cern.ch/record/941318/>. Cited on pages 3 and 4.
- 1036 [7] W. E. Burcham and M. Jobes. *Nuclear and Particle Physics*. Pearson educa-
1037 tion, second edition, 1995. Cited on page 4.
- 1038 [8] The ATLAS Collaboration. Observation of a new particle in the search
1039 for the Standard Model Higgs boson with the ATLAS detector at the LHC.
1040 *Phys. Lett. B*, 716(arXiv:1207.7214. CERN-PH-EP-2012-218):1–29. 39 p,
1041 Aug 2012. Cited on page 4.
- 1042 [9] Serguei Chatrchyan et al. Observation of a new boson at a mass of 125 GeV
1043 with the CMS experiment at the LHC. *Phys.Lett.*, B716:30–61, 2012. doi:
1044 10.1016/j.physletb.2012.08.021. Cited on page 4.
- 1045 [10] Standard model of elementary particles. [http://en.wikipedia.org/](http://en.wikipedia.org/wiki/File:Standard_Model_of_Elementary_Particles.svg)
1046 [wiki/File:Standard_Model_of_Elementary_Particles.svg](http://en.wikipedia.org/wiki/File:Standard_Model_of_Elementary_Particles.svg),
1047 2014. Accessed: 2014-03-24. Cited on page 5.
- 1048

- [11] G. Jungman, M. Kamionkowski, and K. Griest. Supersymmetric dark matter. *Physics Reports*, 267:195–373, March 1996. doi: 10.1016/0370-1573(95)00058-5. Cited on pages 4 and 7.
- [12] V. Trimble. Existence and nature of dark matter in the universe. *Annual Review of Astronomy and Astrophysics*, 25(1):425–472, 1987. doi: 10.1146/annurev.aa.25.090187.002233. URL <http://dx.doi.org/10.1146/annurev.aa.25.090187.002233>. Cited on page 5.
- [13] F. Zwicky. Die Rotverschiebung von extragalaktischen Nebeln. *Helvetica Physica Acta*, 6:110–127, 1933. Cited on page 6.
- [14] NASA. NASA’s solar system exploration: the planets: orbits and physical characteristics. <https://solarsystem.nasa.gov/planets/charchart.cfm>, 2014. Accessed: 2014-03-21. Cited on page 6.
- [15] T. S. van Albada, J. N. Bahcall, K. Begeman, and R. Sancisi. Distribution of dark matter in the spiral galaxy NGC 3198. *Astrophysical Journal*, 295: 305–313, August 1985. doi: 10.1086/163375. Cited on page 6.
- [16] P. Gondolo. Non-baryonic dark matter. *NATO Sci.Ser.II*, 187:279–333, 2005. Cited on page 6.
- [17] J. Goodman, M. Ibe, A. Rajaraman, W. Shepherd, Tim M.P. Tait, et al. Constraints on Light Majorana dark Matter from Colliders. *Phys.Lett.*, B695: 185–188, 2011. doi: 10.1016/j.physletb.2010.11.009. Cited on page 7.
- [18] ATLAS Collaboration. Search for dark matter candidates and large extra dimensions in events with a jet and missing transverse momentum with the atlas detector. *J. High Energy Phys.*, 04(arXiv:1210.4491. CERN-PH-EP-2012-210):075. 58 p, October 2012. URL <http://cds.cern.ch/record/1485031>. Cited on pages 7 and 9.
- [19] J. Goodman, M. Ibe, A. Rajaraman, W. Shepherd, T. M. P. Tait, and H.-B. Yu. Constraints on dark matter from colliders. *Phys.Rev.D*82:116010,2010, 82 (11):116010, December 2010. doi: 10.1103/PhysRevD.82.116010. Cited on page 7.
- [20] ATLAS. Atlas luminosity public results. <https://twiki.cern.ch/twiki/bin/view/AtlasPublic/LuminosityPublicResults>, 2013. Accessed: 2014-03-06. Cited on page 10.
- [21] AC Team. The four main LHC experiments, Jun 1999. URL <http://cds.cern.ch/record/40525>. Cited on page 10.
- [22] The ATLAS Collaboration. The atlas experiment at the cern large hadron collider. *Journal of Instrumentation*, 3(08):S08003. 437 p, 2008. URL <https://cdsweb.cern.ch/record/1129811/>. Cited on page 11.
- [23] J. Pequeno. Computer generated image of the whole ATLAS detector, Mar 2008. URL <http://cds.cern.ch/record/1095924>. Cited on page 12.

- [24] ATLAS Collaboration. Event display for one of the monojet candidates in the data. The event has a jet with $pt = 602$ GeV at $\eta = -1$ and $\phi = 2.6$, $MET = 523$ GeV, and no additional jet with $pt_{jet} > 30$ GeV in the final state. . https://atlas.web.cern.ch/Atlas/GROUPS/PHYSICS/CONFNOTES/ATLAS-CONF-2011-096/fig_08.png, 2011. Accessed: 2014-03-28. Cited on page 13.
- [25] ATLAS Collaboration. Physics at a High-Luminosity LHC with ATLAS. Jul 2013. URL <https://cds.cern.ch/record/1564937>. Cited on page 15.
- [26] J. Alwall, M. Herquet, F. Maltoni, O. Mattelaer, and T. Stelzer. MadGraph 5: going beyond. *Journal of High Energy Physics*, 6:128, June 2011. doi: 10.1007/JHEP06(2011)128. Cited on pages 15 and 33.
- [27] T. Gleisberg, S. Hoeche, F. Krauss, A. Schalicke, S. Schumann, et al. SHERPA 1. alpha: A Proof of concept version. *JHEP*, 0402:056, 2004. doi: 10.1088/1126-6708/2004/02/056. Cited on page 15.
- [28] T. Sjöstrand, S. Mrenna, and P. Skands. A brief introduction to {PYTHIA} 8.1. *Computer Physics Communications*, 178(11):852 – 867, 2008. ISSN 0010-4655. doi: <http://dx.doi.org/10.1016/j.cpc.2008.01.036>. URL <http://www.sciencedirect.com/science/article/pii/S0010465508000441>. Cited on pages 15 and 33.
- [29] The ROOT Team. Root. <http://root.cern.ch/drupal/>, 2014. Accessed: 2014-03-28. Cited on page 15.
- [30] S. Agostinelli, J. Allison, K. Amako, et al. Geant4—a simulation toolkit. *Nuclear Instruments and Methods in Physics Research Section A: Accelerators, Spectrometers, Detectors and Associated Equipment*, 506(3):250 – 303, 2003. ISSN 0168-9002. doi: [http://dx.doi.org/10.1016/S0168-9002\(03\)01368-8](http://dx.doi.org/10.1016/S0168-9002(03)01368-8). URL <http://www.sciencedirect.com/science/article/pii/S0168900203013688>. Cited on page 17.
- [31] ATLAS Collaboration. Performance assumptions for an upgraded ATLAS detector at a High-Luminosity LHC. Mar 2013. URL <https://cds.cern.ch/record/1527529/>. Cited on pages 17, 18, 19, 21, 27, and 28.
- [32] ATLAS Collaboration. Electron performance measurements with the ATLAS detector using the 2010 LHC proton-proton collision data. *Eur. Phys. J. C*, 72(arXiv:1110.3174. CERN-PH-EP-2011-117):1909. 45 p, Oct 2011. Comments: 33 pages plus author list (45 pages total), 24 figures, 12 tables, submitted to Eur. Phys. J. C. Cited on pages 27 and 28.
- [33] ATLAS Collaboration. Search for New Phenomena in Monojet plus Missing Transverse Momentum Final States using 10fb-1 of pp Collisions at $\sqrt{s}=8$ TeV with the ATLAS detector at the LHC. Nov 2012. URL <http://cds.cern.ch/record/1493486/>. Cited on pages 32, 33, 34, 36, 37, and 43.

Upphovsrätt

Detta dokument hålls tillgängligt på Internet — eller dess framtida ersättare — under 25 år från publiceringsdatum under förutsättning att inga extraordinära omständigheter uppstår.

Tillgång till dokumentet innebär tillstånd för var och en att läsa, ladda ner, skriva ut enstaka kopior för enskilt bruk och att använda det oförändrat för icke-kommersiell forskning och för undervisning. Överföring av upphovsrätten vid en senare tidpunkt kan inte upphäva detta tillstånd. All annan användning av dokumentet kräver upphovsmannens medgivande. För att garantera äktheten, säkerheten och tillgängligheten finns det lösningar av teknisk och administrativ art.

Upphovsmannens ideella rätt innefattar rätt att bli nämnd som upphovsman i den omfattning som god sed kräver vid användning av dokumentet på ovan beskrivna sätt samt skydd mot att dokumentet ändras eller presenteras i sådan form eller i sådant sammanhang som är kränkande för upphovsmannens litterära eller konstnärliga anseende eller egenart.

För ytterligare information om Linköping University Electronic Press se förlagets hemsida <http://www.ep.liu.se/>

Copyright

The publishers will keep this document online on the Internet — or its possible replacement — for a period of 25 years from the date of publication barring exceptional circumstances.

The online availability of the document implies a permanent permission for anyone to read, to download, to print out single copies for his/her own use and to use it unchanged for any non-commercial research and educational purpose. Subsequent transfers of copyright cannot revoke this permission. All other uses of the document are conditional on the consent of the copyright owner. The publisher has taken technical and administrative measures to assure authenticity, security and accessibility.

According to intellectual property law the author has the right to be mentioned when his/her work is accessed as described above and to be protected against infringement.

For additional information about the Linköping University Electronic Press and its procedures for publication and for assurance of document integrity, please refer to its www home page: <http://www.ep.liu.se/>